PSEG Nuclear LLC
P.O. Box 236, Hancocks Bridge, New Jersey 08038-0236

PSEG
Nuclear LLC

10 CFR 50.90

LR-N07-0298
LCR H05-01, Rev. 1
November 30, 2007

U.S. Nuclear Regulatory Commission
ATTN: Document Control Desk
Washington, DC 20555-0001

Hope Creek Generating Station
Facility Operating License No. NPF-57
NRC Docket No. 50-354

Subject: Response to Request for Additional Information
Request for License Amendment - Extended Power Uprate

References: 1) Letter from George P. Barnes (PSEG Nuclear LLC) to USNRC, September 18, 2006
2) Letter from USNRC to William Levis (PSEG Nuclear LLC), November 13, 2007

In Reference 1, PSEG Nuclear LLC (PSEG) requested an amendment to Facility Operating License NPF-57 and the Technical Specifications (TS) for the Hope Creek Generating Station (HCGS) to increase the maximum authorized power level to 3840 megawatts thermal (MWt).

In Reference 2, the NRC requested additional information concerning PSEG's request. Attachment 1 to this letter provides responses to the questions with the exception of RAI 14.66 followup. As noted in Reference 2, PSEG will provide the response to this question in a separate transmittal.

PSEG has determined that the information contained in this letter and attachments does not alter the conclusions reached in the 10CFR50.92 no significant hazards analysis previously submitted.

A001
NRR

Attachment 1 contains information proprietary to Continuum Dynamics, Inc. (C.D.I.). C.D.I. requests that the proprietary information in Attachment 1 be withheld from public disclosure in accordance with 10 CFR 2.390(a)(4). An affidavit supporting this request is included with Attachment 1. A non-proprietary version of PSEG's Attachment 1 responses is provided in Attachment 2.

C.D.I. Report 04-09P, "Methodology to Determine Unsteady Pressure Loading on Components in Reactor Steam Domes," is provided in Attachment 3 to this letter. C.D.I. Report 04-09P contains information which C.D.I. considers to be proprietary. C.D.I. requests that the proprietary information be withheld from public disclosure in accordance with 10 CFR 2.390(a)(4). An affidavit supporting this request is provided in Attachment 3. A non-proprietary version of the C.D.I. report is provided in Attachment 4.

There are no regulatory commitments contained within this letter.

Should you have any questions regarding this submittal, please contact Mr. Paul Duke at 856-339-1466.

I declare under penalty of perjury that the foregoing is true and correct.

Executed on 11/30/07
(date)

Sincerely,

George P. Barnes

George P. Barnes
Site Vice President
Hope Creek Generating Station

Attachments
1. Response to Request for Additional Information (proprietary)
2. Response to Request for Additional Information (non-proprietary)
3. C.D.I. Report 04-09P
4. C.D.I. Report 04-09NP

cc: S. Collins, Regional Administrator – NRC Region I
J. Shea, Project Manager - USNRC
NRC Senior Resident Inspector - Hope Creek
P. Mulligan, Manager IV, NJBNE

Continuum Dynamics, Inc.
(609) 538-0444 (609) 538-0464 fax 34 Lexington Avenue Ewing, NJ 08618-2302

AFFIDAVIT

Re: Hope Creek Generating Station – Request for Additional Information Regarding Request for Extended Power Uprate (TAC NO. MD3002)

I, Alan J. Bilanin, being duly sworn, depose and state as follows:

1. I hold the position of President and Senior Associate of Continuum Dynamics, Inc. (hereinafter referred to as C.D.I.), and I am authorized to make the request for withholding from Public Record the Information contained in the documents described in Paragraph 2. This Affidavit is submitted to the Nuclear Regulatory Commission (NRC) pursuant to 10 CFR 2.390(a)(4) based on the fact that the attached information consists of trade secret(s) of C.D.I. and that the NRC will receive the information from C.D.I. under privilege and in confidence.

2. The Information sought to be withheld, as transmitted to PSEG Nuclear LLC as attachment to C.D.I. Letter No. 07220 dated 30 November 2007 Hope Creek Generating Station – Request for Additional Information Regarding Request for Extended Power Uprate (TAC NO. MD 3002).

3. The Information summarizes:

   (a) a process or method, including supporting data and analysis, where prevention of its use by C.D.I.'s competitors without license from C.D.I. constitutes a competitive advantage over other companies;
   (b) Information which, if used by a competitor, would reduce his expenditure of resources or improve his competitive position in the design, manufacture, shipment, installation, assurance of quality, or licensing of a similar product;
   (c) Information which discloses patentable subject matter for which it may be desirable to obtain patent protection.

   The information sought to be withheld is considered to be proprietary for the reasons set forth in paragraphs 3(a), 3(b) and 3(c) above.

4. The Information has been held in confidence by C.D.I., its owner. The Information has consistently been held in confidence by C.D.I. and no public disclosure has been made and it is not available to the public. All disclosures to third parties, which have been limited, have been made pursuant to the terms and

conditions contained in C.D.I.'s Nondisclosure Secrecy Agreement which must be fully executed prior to disclosure.

5. The Information is a type customarily held in confidence by C.D.I. and there is a rational basis therefore. The Information is a type, which C.D.I. considers trade secret and is held in confidence by C.D.I. because it constitutes a source of competitive advantage in the competition and performance of such work in the industry. Public disclosure of the Information is likely to cause substantial harm to C.D.I.'s competitive position and foreclose or reduce the availability of profit-making opportunities.

I declare under penalty of perjury that the foregoing affidavit and the matters stated therein are true and correct to be the best of my knowledge, information and belief.

Executed on this 30th day of NOVEMBER 2007.

Alan J. Bilanin
Continuum Dynamics, Inc.

Subscribed and sworn before me this day: NOV. 30, 2007

Eileen P. Burmeister, Notary Public

EILEEN P. BURMEISTER
NOTARY PUBLIC OF NEW JERSEY
MY COMM. EXPIRES MAY 6, 2012

ATTACHMENT 2

Hope Creek Generating Station

Facility Operating License NPF-57
Docket No. 50-354

Extended Power Uprate
Response to Request for Additional Information

In Reference 1, PSEG Nuclear LLC (PSEG) requested an amendment to Facility Operating License NPF-57 and the Technical Specifications (TS) for the Hope Creek Generating Station (HCGS) to increase the maximum authorized power level to 3840 megawatts thermal (MWt).

In Reference 2, the NRC requested additional information concerning PSEG's request. PSEG's responses are provided below.

14. Mechanical & Civil Engineering Branch

RAI 14.77 Follow-up

In RAI 14.77, PSEG was requested to provide the following information for the seven weld locations, identified in Table 7b of CDI Report No. 06-27 (Rev. 2), having minimum alternate stress ratio (SR-a) at 115 percent current licensed thermal power (CLTP) conditions with frequency shifts: (1) thickness of the plates at a weld location, (2) if thicknesses are different, identify the nominal stresses in the weld leg attached to the thicker plate, (3) identify the type of loading (normal or bending) acting on the weld during EPU operation, (4) estimate the undersize weld factors, and (5) estimate the minimum alternate stress ratio at the seven weld locations taking into account the undersize weld factors. PSEG has provided part of the requested information in a table for six weld locations where components of different thicknesses are connected.

As a follow-on to RAI 14.77, the licensee is requested to provide the following missing information for each of the six weld locations: (1) identify the alternating stress intensity in both thick and thin components; (2) identify the type of loading (normal and/or bending) acting on the weld; (3) estimate the corresponding undersize weld factors; and (4) estimate the alternate stress ratio for both thick and thin plates.

Response
In addition to the requested information, PSEG has provided some technical discussions of the consequences of using undersize weld factors for connections with properly sized welds. An inspection was performed of the Hope Creek Unit 2 dryer and it was concluded that the welds are properly sized. As previously discussed the Unit 1 dryer is identical to Unit 2 with the exception that some connections were strengthened

on the Unit 1 dryer. It is therefore reasonable to conclude that the welds on the Unit 1 dryer are also properly sized.

Our response is broken down into two parts. The first is a discussion of how the Under Sized Weld Factors (USWF) are calculated, the second is the presentation of the requested information.

The discussion of the USWF calculation includes clarification on what is meant by an undersize weld. This point is essential. When welding together dissimilar thickness components the appropriate size of weld leg is the thickness of the thinner component.
[[

[redacted]

[redacted]

(3)]]

Table RAI14.77.1. Original and modified stress intensities for selected nodes listed in Table 7b of CDI Report 06-27, Rev. 2.

[[

[redacted]

(3)]]

Notes:

1. This thicker member forms the horizontal component of the T-junction. For these members no undersize weld factor should be used since the weld stress is governed by the stresses in the vertical leg of the T-junction.
2. This thicker member forms the vertical leg of the T-junction. For these members the undersize weld factor used for bending stresses is $\beta=3\alpha^2/(1+2\alpha)$.
3. The last column reports the stress ratios reported in Table 7b of CDI Report 06-27, Rev. 2.
4. Stress Intensities are a combination of normal and bending loads.
5. [[

[(3)]]

Conclusion

The welds on the Hope Creek dryer are appropriately sized. Application of an USWF results in an over conservative estimate of the stresses at the connection.

[[

(3)]]

RAI 14.79 Follow-up

In response to RAI 14.79 and in Section 3.8, *Mesh Details and Element Types*, of CDI Report No. 07-17P, PSEG describes numerical experiments carried out using the ANSYS code applied to simple analytically tractable structures with dimensions and mesh spacing similar to the ones used for the steam dryer, confirming that the natural frequencies are accurately recovered (less than 1 percent errors for the first modes). The staff noted that establishing convergence of resonance frequencies is not sufficient to establish convergence of strain and stress fields. Also, frequency shifting loading functions does not account for lack of convergence in strain and stress fields. Therefore, as a follow-up to RAI 14.79, PSEG is requested to provide pertinent parametric evaluations related to mesh convergence in high strain and stress regions in the Hope Creek steam dryer to assess whether the dimensions and mesh spacing used for the model are adequate. In particular, plots of stresses near high stress regions for coarse and dense FE meshes could be used to confirm that the dryer model used to establish the Hope Creek limit curves are converged.

Response

Mesh refinement tests were conducted on a structure excised from the Hope Creek Unit 1 steam dryer comprising the middle hood with two hood supports, side plate, cover plates and closure plate as shown in Figure RAI14.79.1. All dimensions and structural properties were kept the same as in the full model. Structural damping was prescribed at 1% of critical at all frequencies. Cantilevered supports were introduced at the edges typically coupled to heavier parts of the steam dryer such as the upper support ring and vane bank.

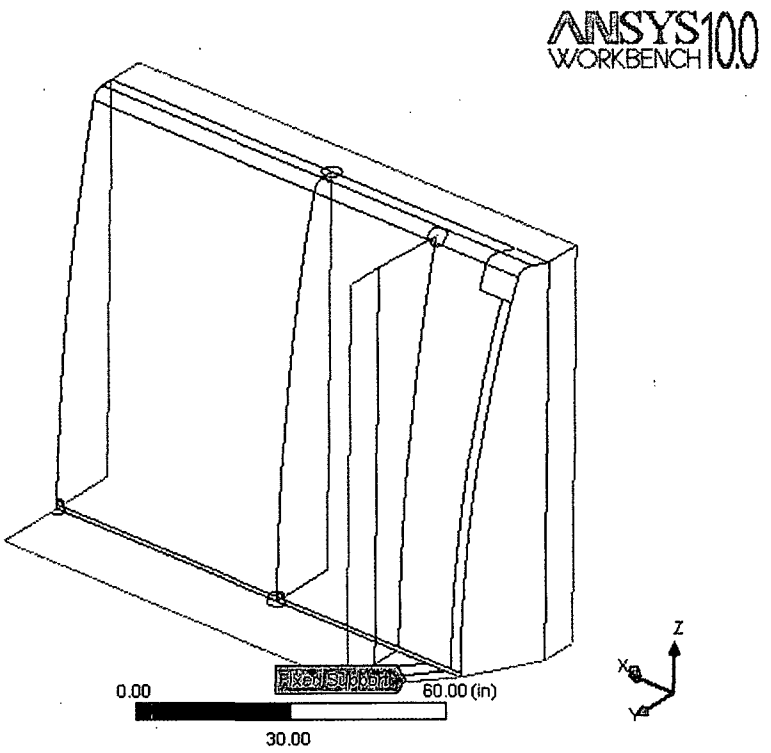

Figure RAI14.79.1. Substructure of a steam dryer used for mesh convergence tests. Blue lines indicate cantilevered support, red lines denote free edges, and black lines show connections between parts.

The elements used in the analysis are of the same type as those used in the steam dryer calculations, namely SHELL63 in ANSYS notation. This quadrilateral shell element utilizes Discrete Kirchoff Triangles (DKT) technology, providing cubic interpolation order in the displacement component normal to the shell surface along the edges, and, therefore, quadratic stress variation. Note that contour plots produced by ANSYS are linear over the elements and, thus, are only approximately representative of the stress and displacement variation supported by this element.

The structure in Figure RAI14.79.1 was subjected to loadings characteristic of those present in the actual analysis of the steam dryer. Specifically, the structure was loaded by its own weight for the static component and subjected to the same harmonic pressure distributions applied to the full dryer. Displacements and stresses were computed in the same way as in the full steam dryer stress evaluation.

To investigate the mesh dependence of stresses and displacements, three different grids were considered. The coarsest mesh, labeled Mesh x1, is representative of the mesh sizing used in the full steam dryer calculation (see top figure of Figure RAI14.79.2a) and contains 4329 nodes and 4208 elements. A finer mesh, denoted by Mesh x2 and containing 11914 nodes and 11726 elements, is obtained by uniformly

refining the coarser mesh, resulting in elements that are approximately half the size of Mesh x1. The finest mesh, labeled Mesh x4, contains 54324 nodes and 53912 elements that are approximately four times smaller than in the original Mesh x1. All three grids are shown in Figure RAI14.79.2.

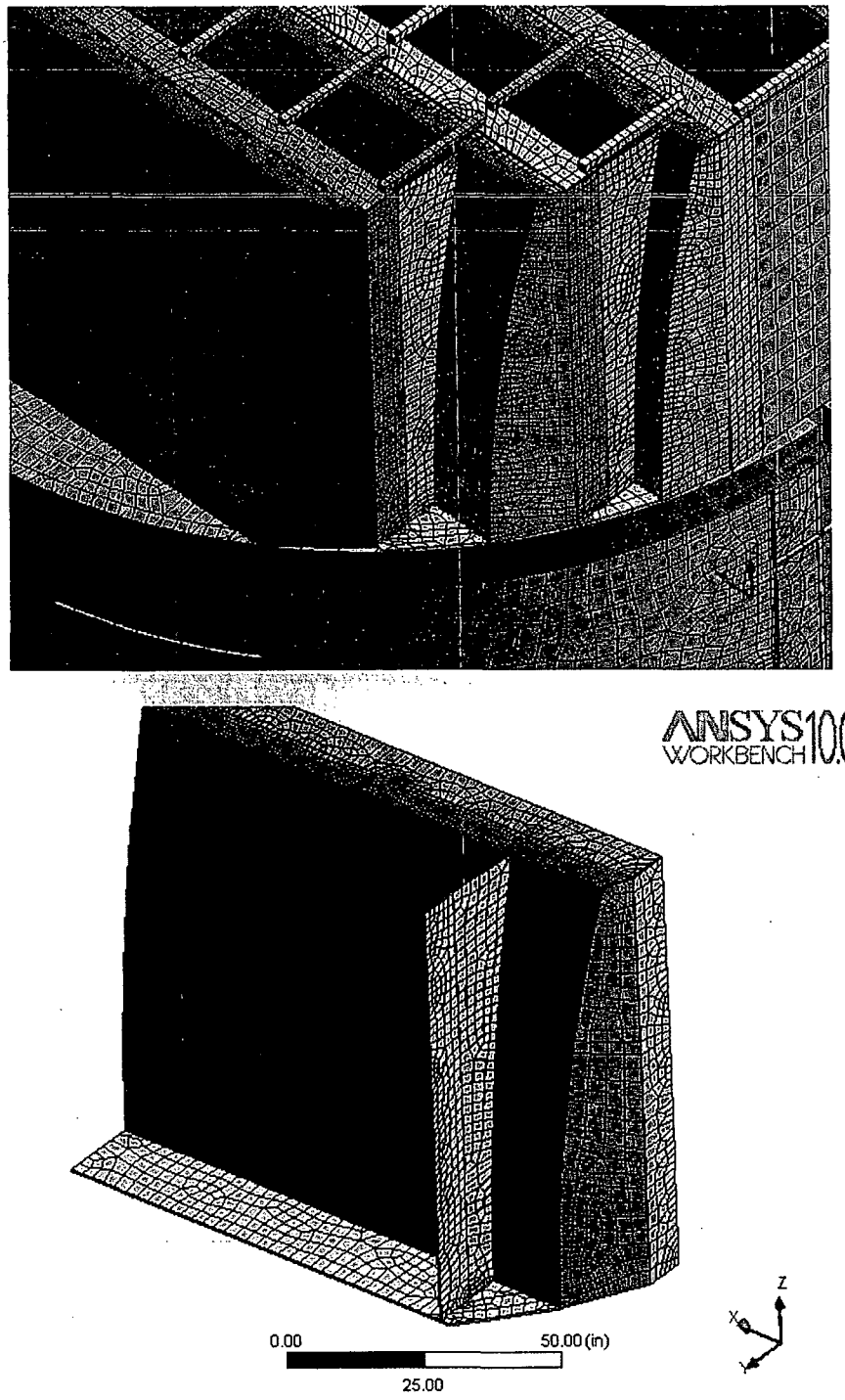

Figure RAI14.79.2a. Mesh used in full steam dryer analysis (top figure) and the coarsest mesh, Mesh x1, used in the convergence tests (bottom figure).

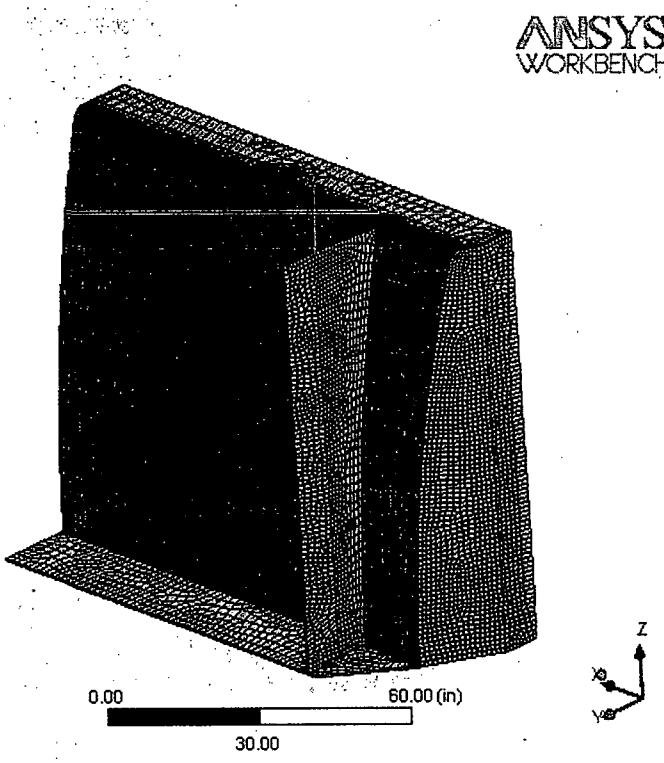

Figure RAI14.79.2b. Refined mesh, denoted Mesh x2.

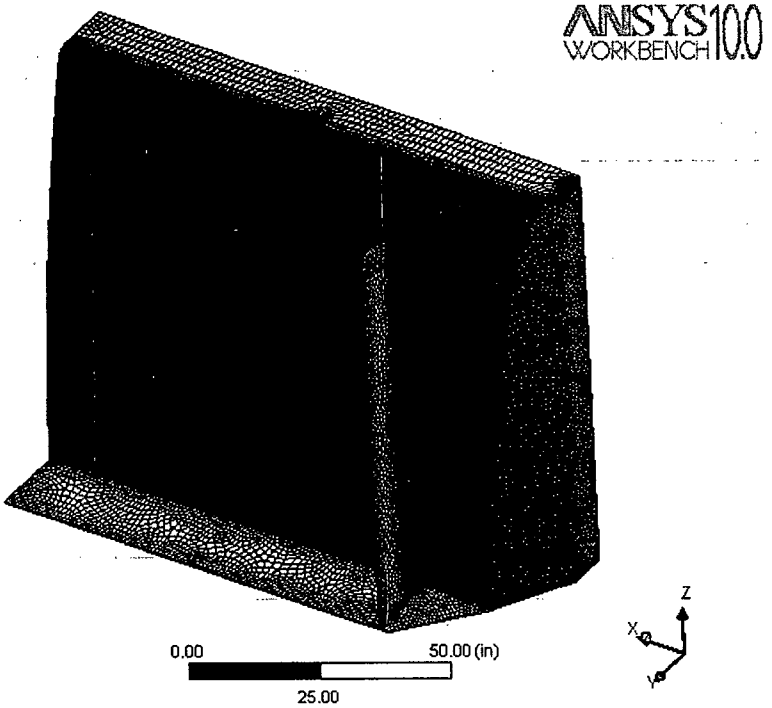

Figure RAI14.79.2c. Further refined mesh, denoted Mesh x4.

Convergence in Static Analysis

The deformations due to gravity were calculated on the three meshes described above. In addition, deflections and stresses were also calculated on grids refined locally using the adaptive meshing capability provided by the ANSYS Simulation module. This adaptive refinement is performed automatically by ANSYS in locations where higher discretization error is detected. This additional refinement was performed on each mesh except Mesh x4, where further adaptive refinement was not needed because the element size was already very small.

The typical convergence behavior for the maximum stress intensity during adaptive mesh refinement is shown in Figure RAI14.79.3, where the horizontal scale ("Iteration Number") is the number of adaptive mesh refinement steps. The results of adaptive refinement for all three initial grids are summarized in Table RAI14.79.1. The calculated stresses did not change appreciably during adaptive local mesh refinement. Overall, the range of computed stress intensity values is within 4% of stress intensity values computed on Mesh x1. The deflected shapes and stress intensity distributions are shown in Figure RAI14.79.4. These results show that the static solution is indeed satisfactorily converged on the grid Mesh x1.

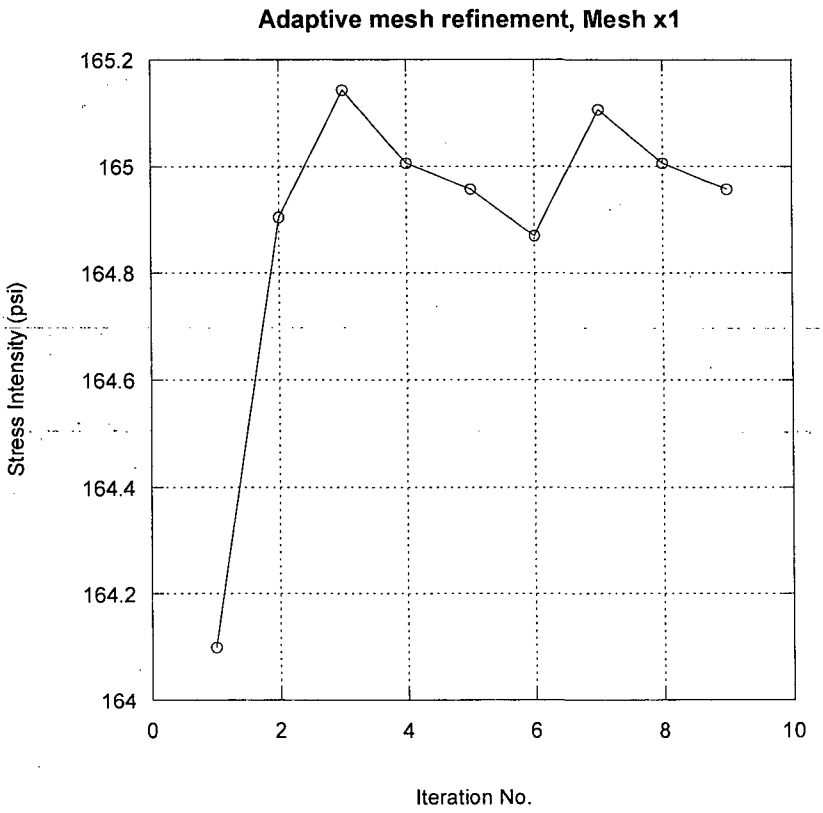

Figure RAI14.79.3. Evolution of stress intensity with adaptive convergence on Mesh x1.

Table RAI14.79.1. Static solution.

Static solution – structure under its own weight			
Mesh	Maximum displacement, in	Maximum stress intensity, psi	Maximum stress intensity after adaptive refinement, psi
Mesh x1	$1.58\ 10^{-3}$	164.10	164.96
Mesh x2	$1.58\ 10^{-3}$	169.37	166.17
Mesh x4	$1.58\ 10^{-3}$	169.37	no adaptation performed

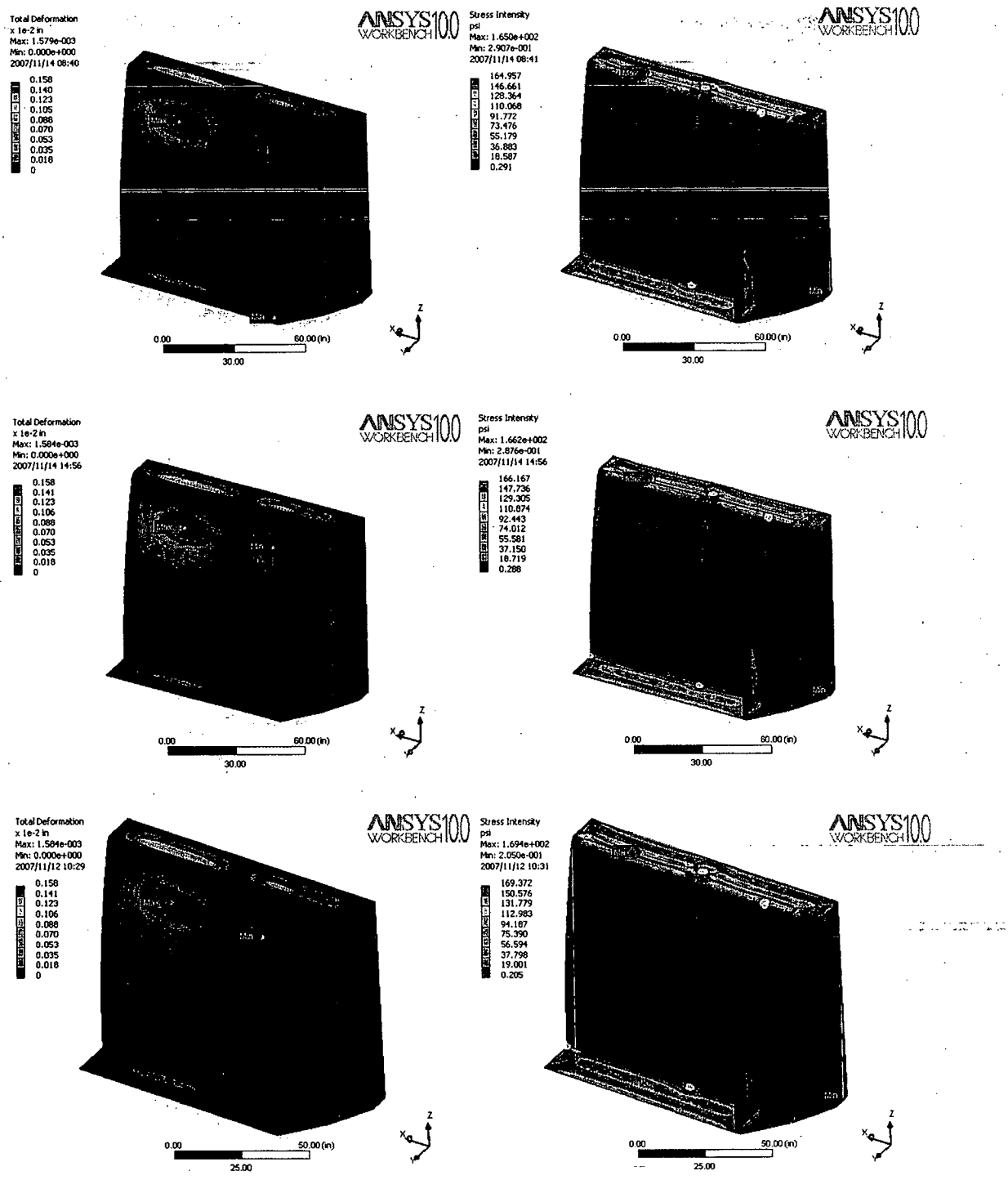

Figure RAI14.79.4. Comparison of static deflections (left side) and stress intensities (right side) for the grids Mesh x1 (top row), Mesh x2 (middle row), and Mesh x4 (bottom row).

Note on "Hot-Spots"

In the stress convergence results, several locations are excluded from the maximum stress evaluation. These locations were identified during adaptive mesh refinement as having non-convergent stress. The typical stress intensity behavior during mesh refinement at these "hot spots" is shown in Figure RAI14.79.5. In Figure RAI14.79.6 a typical stress singularity is shown at the re-entrant corner, created by connection of the top of the closure plate to the hood. Note that several plate thicknesses from the junction, the calculated stresses are low and consistent with overall stress distribution. Such "hot spots" can occur at structural discontinuities, such as re-entrant corners, where the stress becomes infinite as the mesh is refined. For example, a re-entrant corner in a continuum element will generally develop infinite stresses. Likewise, the membrane (in-plane) stresses in a shell or plate will become infinite at re-entrant cutouts or cantilever roots when in-plane loads are applied (bending stresses in shells generally converge).

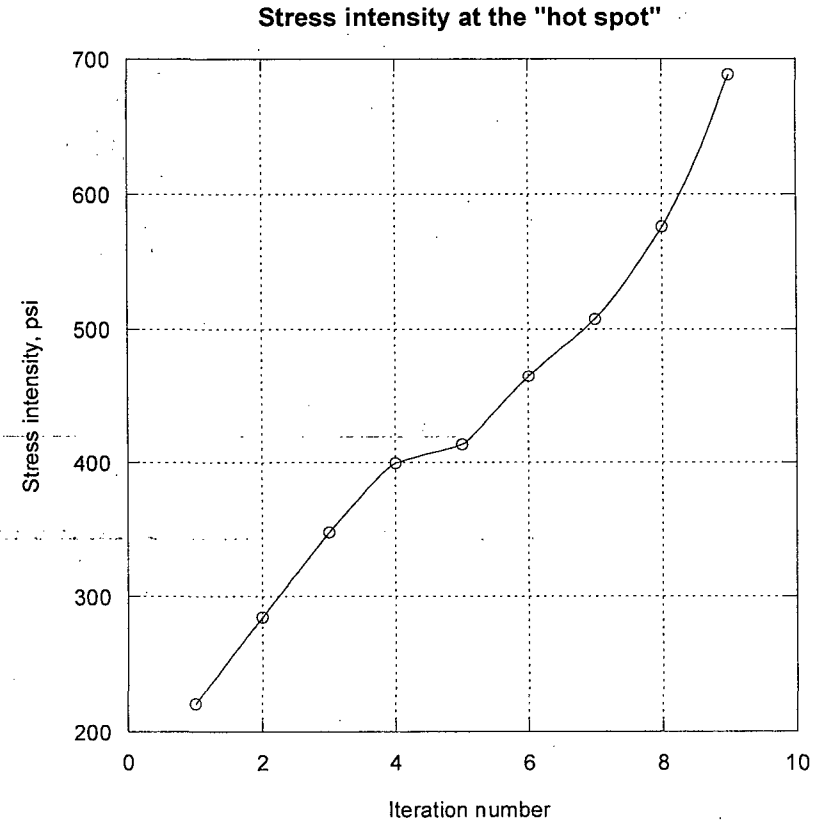

Figure RAI14.79.5. Evolution of stress intensity with adaptive convergence at "hot spot" on Mesh x1.

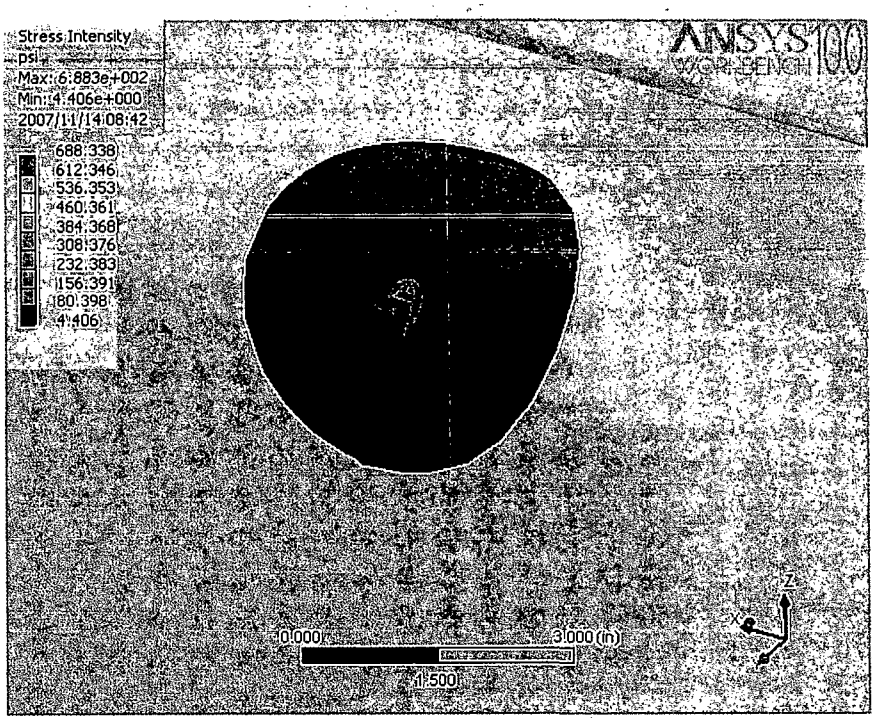

Figure RAI14.79.6. Stress singularity at hood / closure plate junction.

These singular behaviors are mathematically correct and consistent with analytical results. For example, the classic Williams series solution (Williams, M. L., "Stress singularities resulting from various boundary conditions in angular corners of plates in extension," *J. Appl. Mech.*, 74, pg. 526–528, 1952) for the 2D stress field at a corner with notch angle 2γ (γ=0 for a crack), shows that the stress behaves as $O(r^{\lambda-1})$, where λ is obtained from the transcendental equation $\lambda\sin(2\alpha)+\sin(2\lambda\alpha)=0$. Since $\lambda<1$ for $\gamma>\pi/2$, the stress field for a re-entrant notch is locally singular. The study of these singularities is well developed in crack propagation theory with applications to fatigue. The main point to note is that simply refining the mesh of a complex structure will reveal that stresses do *not* (and should not) converge at junctions and corners, but will continue to grow without bound. These "hot spots" are usually very localized, and stresses away from these spots converge to finite limiting values. Even so, resorting to substructuring techniques or adaptive gridding will not necessarily produce global convergence.

This behavior is well known in the structural elasticity community and is addressed in alternate ways. One option is to smooth corners and apply finite fillet radii at various locations. The drawbacks of this approach are that in real life, weld and junction geometries are usually neither known to this level of accuracy nor abide by such smooth radii idealizations (e.g., real welds are uneven and exhibit variability). Another drawback is the huge number of elements required to model every junction and corner at mesh resolutions sufficient for converged stresses. Another option is to extrapolate stresses to junctions from points away from the junction. Popular choices for shell

elements are to evaluate the stress at distances t and 2t away from the junction, where t is the thickness, and extrapolate these stresses to the junction. By fixing the extrapolation points and refining element size, convergence eventually sets in. Again, this approach is only feasible when the structure is relatively simple, so that high resolution can be achieved with manageable element counts. In the present model it is not possible to use elements with spacing on the order of the thickness, since this would produce an enormous number (10 million or more) of finite elements. Moreover, linear extrapolation through two locations is itself an approximation which adds to other approximations such as neglecting 3D effects (which dominate at junctions) and weld variability.

In our approach a conservative and computationally practical approximation described in the ASME code is adopted, where the stresses at welded junctions are estimated using weld factors. These factors account for stress concentration as well as weld variability and are determined from collated experience in the design and operation of welded structures. Accordingly, the peak stresses at junctions and other discontinuities are estimated by evaluating the stresses away from the discontinuities (i.e., the nominal stresses, which will be accurately converged) and multiplying them by the weld factor. In our implementations, a more conservative approach is adopted where the "nominal stresses" are taken as the FEA stresses at the discontinuities rather than a small distance away. Since these junction stresses will generally be somewhat higher (and become infinite with finer mesh size) than those away from the junction, this approach will predict correspondingly higher peak stresses and therefore confer added conservatism.

Convergence in Harmonic Analysis

The full steam dryer stress analysis proceeds by calculating the harmonic structural response at a number of frequencies. The combination of these harmonics and comparison of these assembled solutions with transient simulations is addressed in RAI 14.110. Here the accuracy of the harmonic stress solutions is estimated. To this end, the grids Mesh x1, Mesh x2, and Mesh x4, described above, were again used. The structure was subjected to the same harmonic pressure fields used in the full steam dryer analysis. Specifically, the pressure loading resulting from a unit monopole pressure at the MSL A inlet was applied to the structure. Here the harmonic stresses are examined at the following frequencies: 53.863 Hz, 101.4 Hz and 199.61 Hz. These values were selected from the discrete frequency schedule used in the full steam dryer analysis and chosen to represent the low, medium and high ends of the frequency range. The real parts of the associated pressure fields are shown in Figure RAI14.79.7. Note that both real and imaginary parts of pressure are applied to the structure. Consequently, the calculated stresses and displacements also contain both real and imaginary parts. The vibration amplitudes are given in the usual manner by taking the absolute value of the complex quantities. The stress intensity is computed here by computing the stress intensity, S_r, of the real component of the stress tensor, and the stress intensity, S_i, for the imaginary component. The reported stress intensity for the

node is then given by $S = \sqrt{S_r^2 + S_i^2}$. Note, further, that the "hot spots" identified in the static convergence study are removed from stress evaluation.

For each calculation the nodes having the largest real (Location 1) or imaginary (Location 2) parts in the response were considered. The amplitudes of total displacement and stress intensity were computed and compared on the different grids. The locations of the maximum displacement and stress intensity were the same on all grids, as can be seen from comparison of real and imaginary stress distributions in Figure RAI14.79.8. These plots show that the stress intensity distributions are qualitatively similar on all meshes, and that maximum stresses and displacements occur at the same locations.

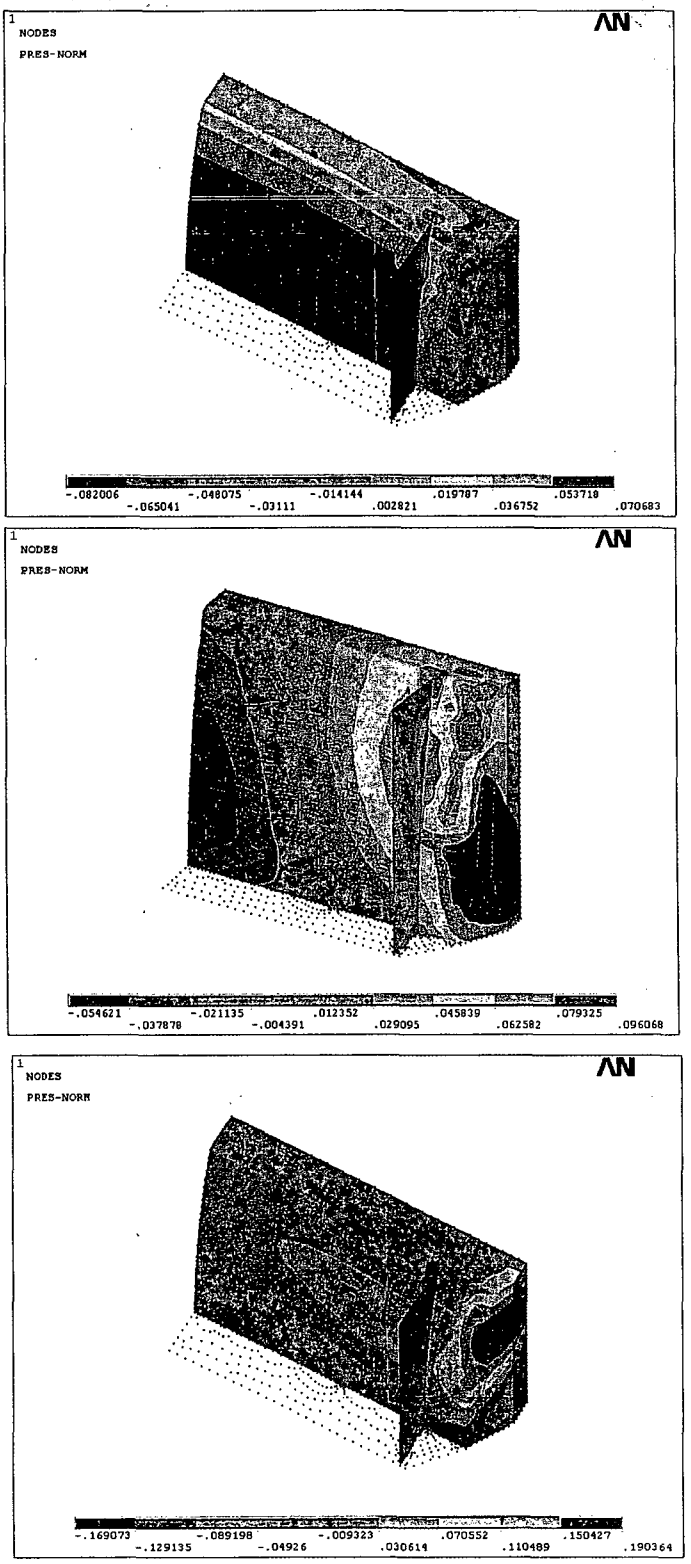

Figure RAI14.79.7. Pressure distribution, real part, at 53.863 Hz (top), 101.4 Hz (middle), and 199.61 Hz (bottom).

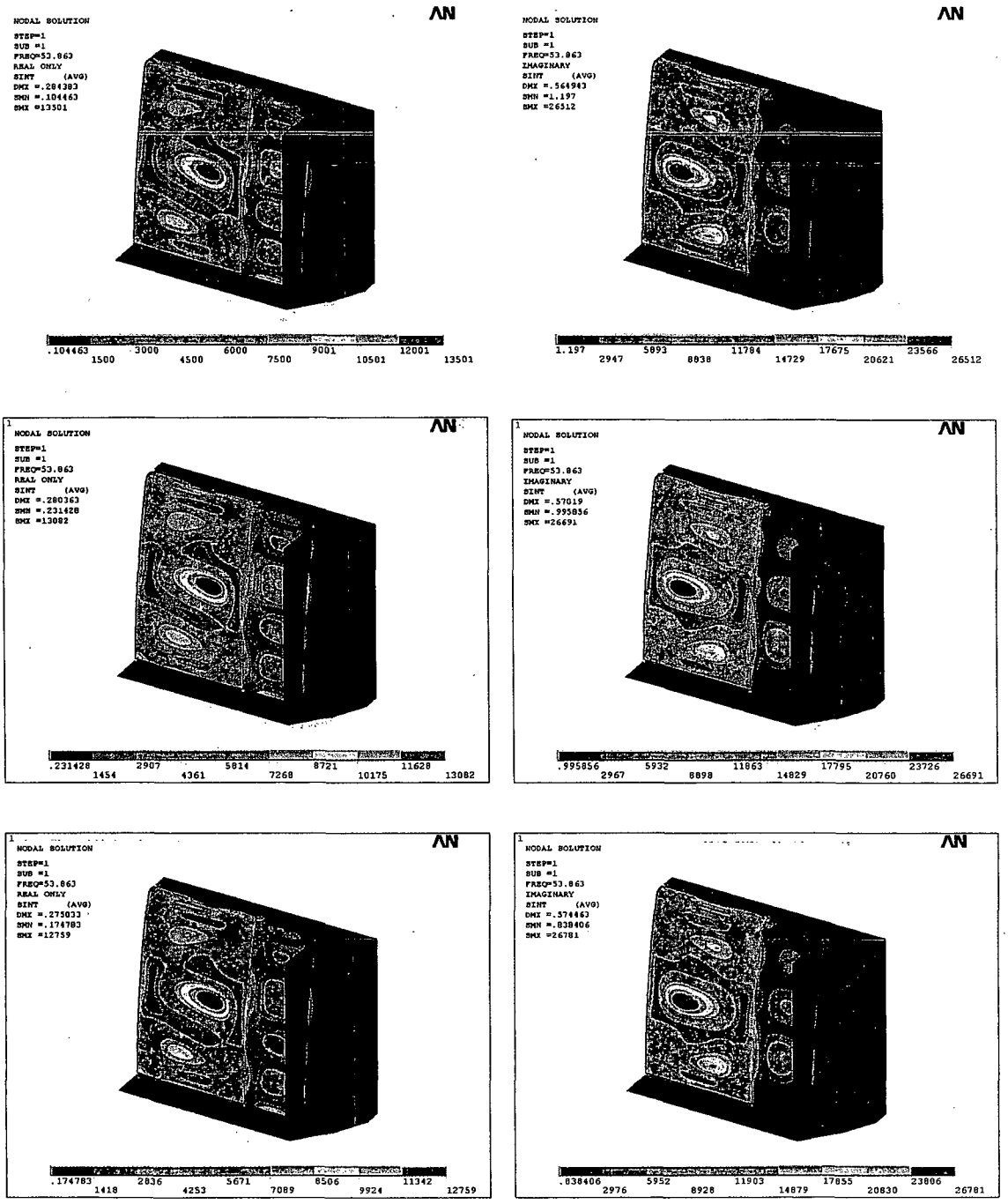

Figure RAI14.79.8a. Comparison of the real (left side) and imaginary (right side) components of the stress intensity distribution at 53.863 Hz on Mesh x1 (top), Mesh x2 (middle), and Mesh x4 (bottom).

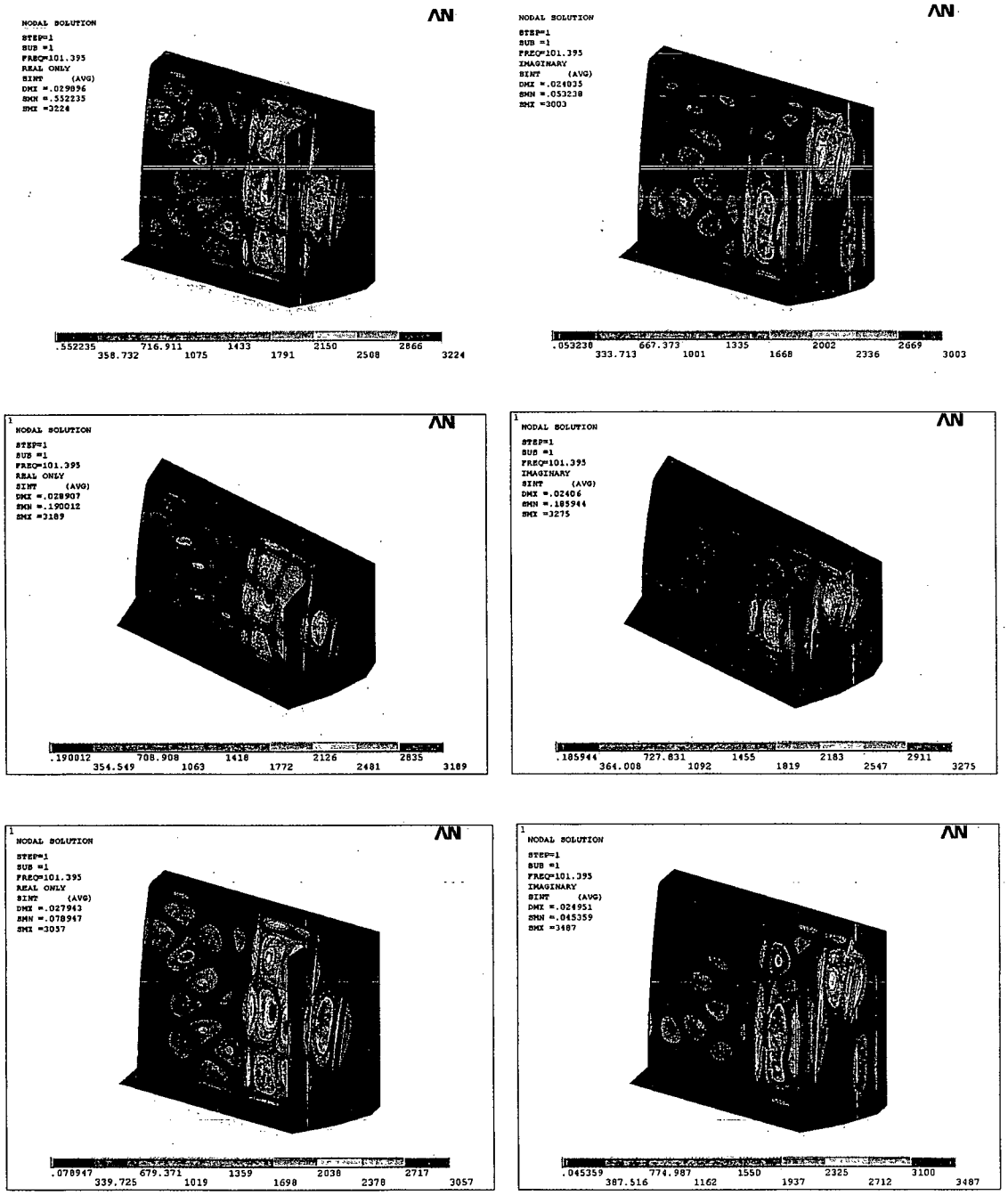

Figure RAI14.79.8b. Comparison of the real (left side) and imaginary (right side) components of the stress intensity distribution at 101.4 Hz on Mesh x1 (top), Mesh x2 (middle), and Mesh x4 (bottom).

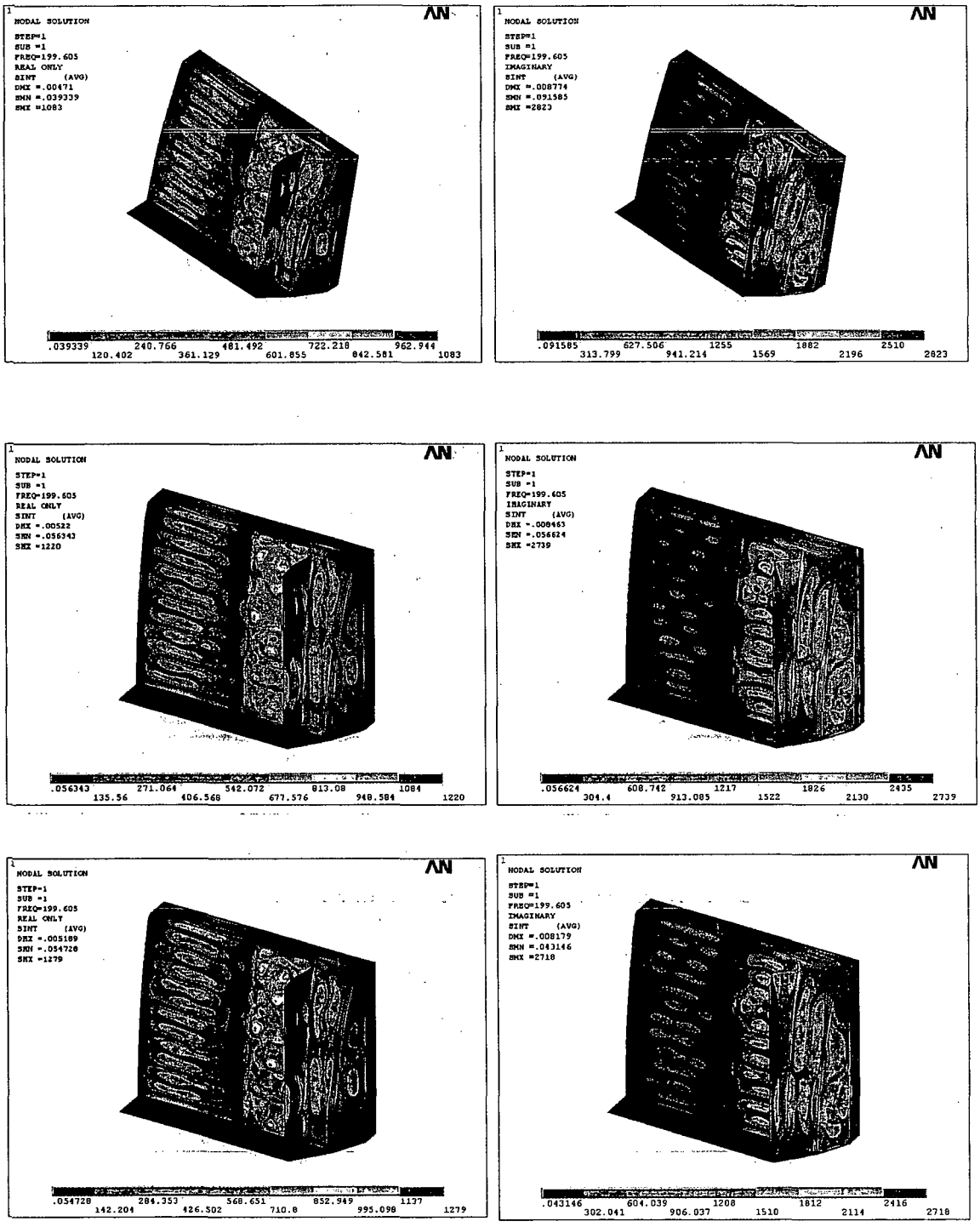

Figure RAI14.79.8c. Comparison of the real (left side) and imaginary (right side) components of the stress intensity distribution at 199.61 Hz on Mesh x1 (top), Mesh x2 (middle), and Mesh x4 (bottom).

In Tables RAI14.79.2 and RAI14.79.3 below, quantitative comparisons of the maximum displacement and stress intensity amplitudes on the three meshes are given. Location 1 corresponds to where the real part of the corresponding solution is a maximum; Location 2 corresponds to maximum imaginary part. These tables show that the displacements and stresses are computed to within 10% uncertainty in the wide range of frequencies, except one location, namely Location 2 at 101.4 Hz where the variation in stress intensity is 15.8%.

Table RAI14.79.2. Total displacement amplitudes of the harmonic solution on different resolution meshes.

	Mesh x1	Mesh x2	Mesh x4	Variation
Frequency 53.863 Hz				
Location 1	0.5265	0.5188	0.5391	3.9%
Location 2	0.6053	0.6095	0.6149	1.6%
Frequency 101.4 Hz				
Location 1	0.0306	0.0304	0.0305	<1%
Location 2	0.0241	0.0241	0.025	3.7%
Frequency 199.61 Hz				
Location 1	0.00693	0.00688	0.00632	9.7%
Location 2	0.00907	0.00896	0.00874	3.8%

Table RAI14.79.3. Total stress intensity amplitudes of the harmonic solution on different resolution meshes.

	Mesh x1	Mesh x2	Mesh x4	Variation
Frequency 53.863 Hz				
Location 1	24328*	23480*	23741*	3.6%
Location 2	28224*	28324*	28490*	<1%
Frequency 101.4 Hz				
Location 1	3272	3296	3255	1.3%
Location 2	3017	3283	3493	15.8%
Frequency 199.61 Hz				
Location 1	1826	1813	1728	5.7%
Location 2	2880	2865	2851	1%

* - Note that the large stress intensities reported in the table correspond to the pressure field resulting from a *unit* (1 psi) pressure fluctuation at the inlet of MSL A. In actual

operation, the pressure fluctuation are much smaller; here at 53.863 Hz the pressure magnitude is only 3×10^{-5} psi. Hence actual stresses will be correspondingly smaller also.

To investigate the reason for this discrepancy, additional calculations were undertaken over the 100 – 102 Hz frequency range in 0.25 Hz increments, and the amplitude at Location 2 was computed. The results are summarized in Figure RAI14.79.9 and show that at 101.4 Hz the frequency response is changing rapidly and that the 15.8% variation can be attributed to the slight shift in the frequency response on different meshes. Thus, rather than comparing the stress intensities at a fixed frequency, it is more useful to compare the maximum stress intensity amplitudes on each mesh. This comprises a more relevant comparison, since these maxima in the stress intensity frequency responses correspond directly to the values tabulated in the full steam dryer stress reports (and, consequently, also the stress ratios). From Figure RAI14.79.9, the peak response on all meshes occurs at 100.75 Hz. The associated peak stress amplitudes are plotted versus mesh size in Figure RAI14.79.10. The actual values are 3510.4 psi on Mesh x1, 3688.5 psi on Mesh x2, and 3790.8 psi on Mesh x4. In Figure RAI14.79.10 the mesh size is normalized by the average element size of Mesh x1; hence the normalized mesh sizes of Mesh x1, Mesh x2, and Mesh x3 are 1.0, 0.5, and 0.25, respectively. It may be seen that computed peak stresses adhere closely to a linear dependence on mesh size. Therefore, one can fit the available values and reliably extrapolate to estimate the stress peak at infinite mesh resolution (i.e., mesh size = 0). From the equation of the linear fit, shown on Figure RAI14.79.10, the best estimate of stress intensity at the peak is 3880 psi. This implies that the error in the coarsest Mesh x1 peak stress prediction (of 3510.4 psi) is (3510.4 – 3880.0)/3880.0 = 9.53%.

Note that for the two other frequencies, 53.863 Hz and 199.61 Hz, the computed stresses show considerably less variation because the excitation is away from resonant peaks, so that the frequency response curves do not exhibit steep slopes about these frequencies.

In conclusion, a grid with element size typical of Mesh x1, which is representative of that used in the full steam dryer evaluation, incurs errors in the peak stresses that are less than 10%.

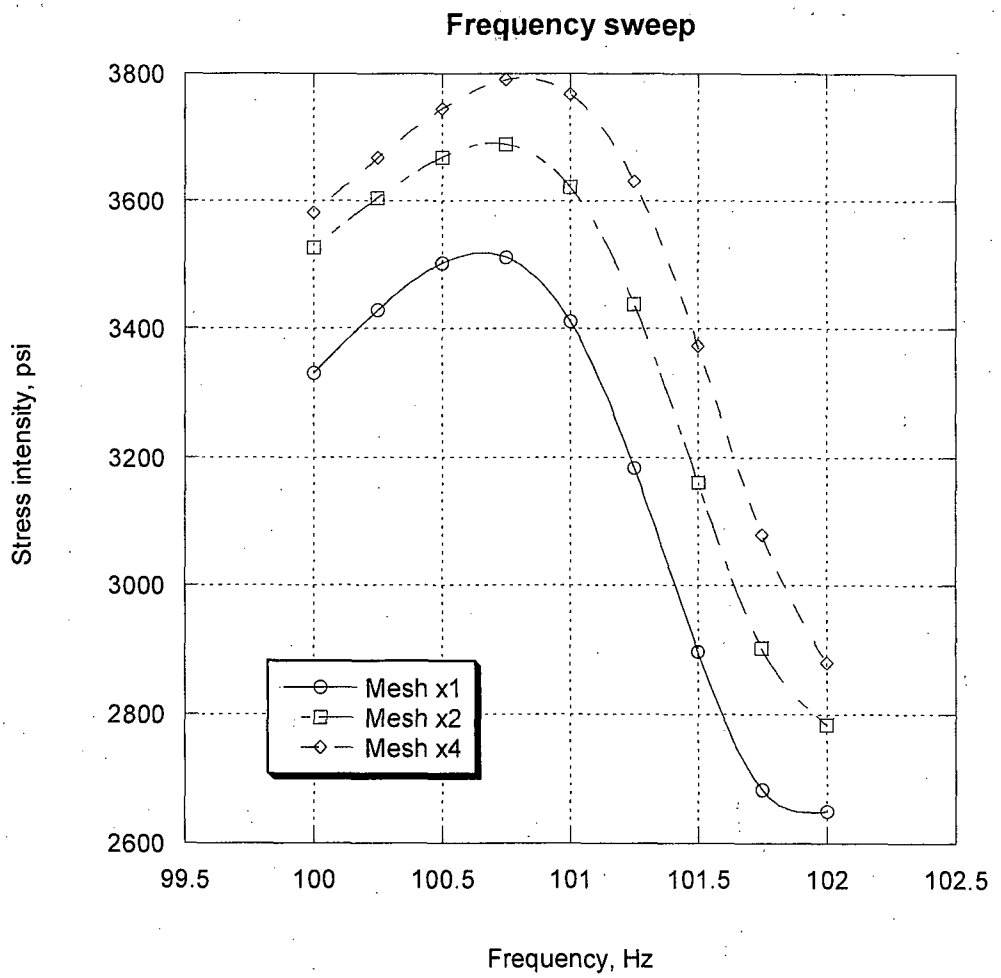

Figure RAI14.79.9. Stress intensity amplitude vs. frequency for Location 2 in the 100 – 102 Hz frequency range.

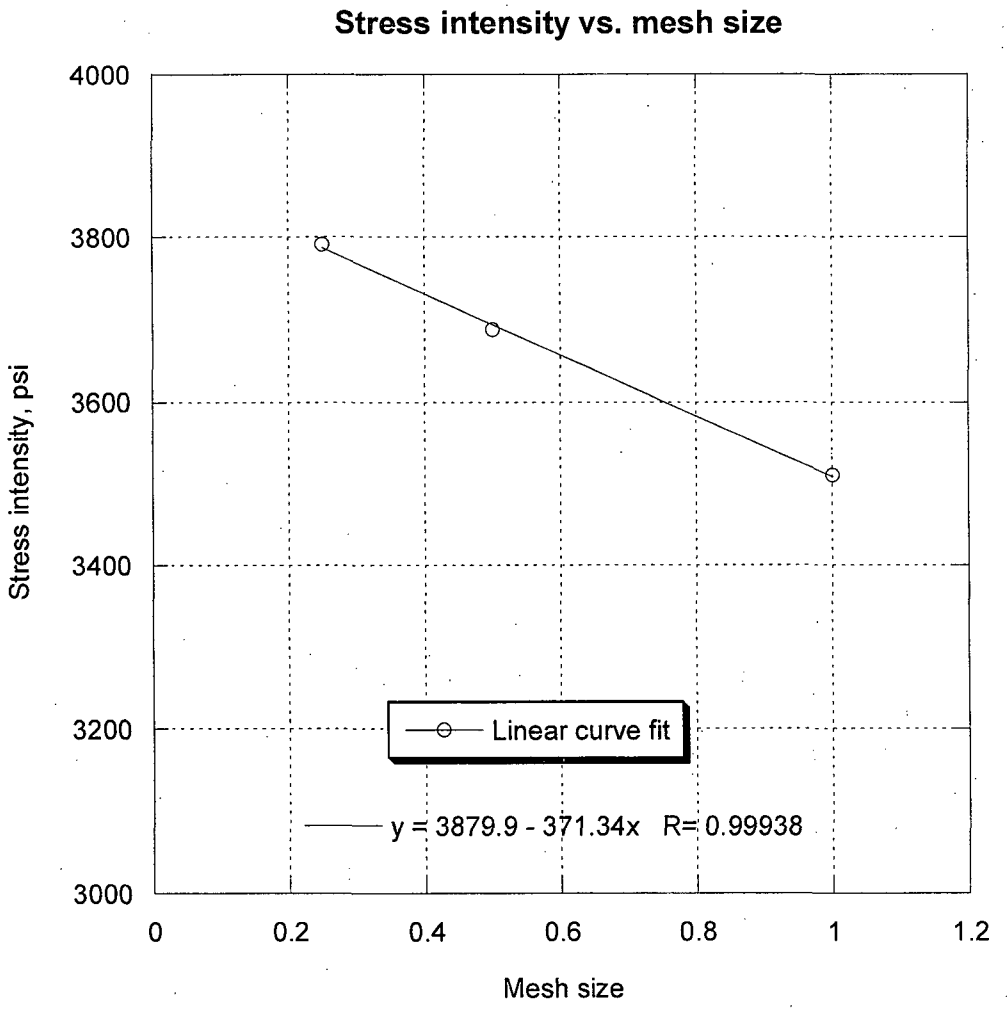

Figure RAI14.79.10. Extrapolation of the peak stress intensity amplitudes as a function of mesh size. The peak stress amplitudes occur at 100.75 Hz in Figure RAI14.79.9. The mesh size is normalized by the mesh spacing on Mesh x1.

RAI 14.107 Follow-up

The projected Hope Creek MSL pressure spectra provided in response to RAI 14.107 show that tones may appear near 120 Hz. Since PSEG currently filters 120 Hz signals from the MSL measurements, explain the monitoring and calculation of stress effects of any valve singing tone that occurs near 120 Hz.

Response

The anticipated standpipe excitation frequency is 118 Hz. Electrical noise exhibits itself in the main steam line pressure data as narrow spikes centered on 60, 120, and 180 Hz shown by the blue curve in Figure RAI14.107.1. When these frequency spikes are processed by a MatLab function that uses a second-order stop-band Butterworth filter, the original signal is not affected outside of a frequency width of ± 1.0 Hz.

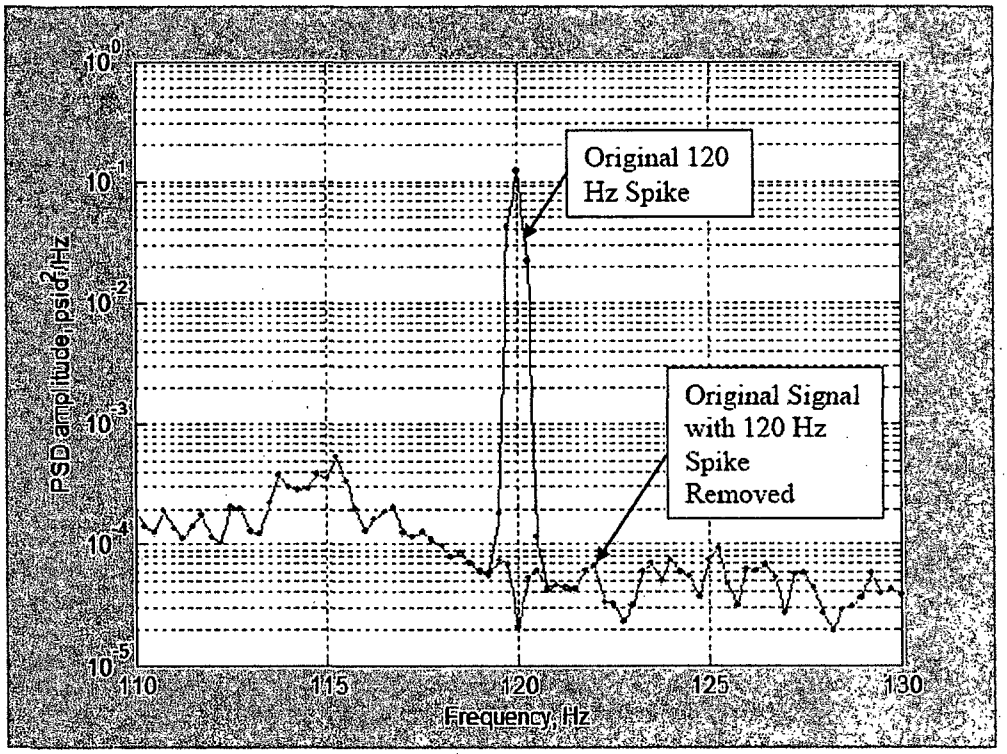

Figure RAI14.107.1. MatLab comparison between an unfiltered signal (blue curve) and a narrow filtered signal (green curve) around 120 Hz.

[[

(3)]] A sample of this raw data from main steam line A is shown in Figure 14.107-2. It would be difficult for this feature to mask a flow induced vibration signal, which has a frequency width that is typically three or four times wider based on industry experience. See for instance C.D.I. Report No. 07-09P, Figure 6.1.

[[

Figure 14.107-2: [[ ]]

RAI 14.110 Follow-up

The stress analysis of the Hope Creek steam dryer represents the first application of the frequency based approach as presented in CDI Report 07-17P for [[

]]. Therefore, a comprehensive verification of this approach is necessary for the reliable prediction of stresses in the Hope Creek steam dryer. The [[

]]. To validate the approach, a rigorous calculation that includes (1) a complex structural dynamic FE model, and (2) a complex spatial and temporal surface loading, is necessary. Item (1) has been met by the existing calculation, but item (2) has not. PSEG notes that [[

]] when analyzing a full steam dryer model. PSEG could consider an alternative analysis to verify the new approach. For example, a small section of a steam dryer could be analyzed, such as one of the outer hoods, using actual plant loads (such as those from CDI report 07-17P) over all frequencies. The outer hood boundaries could be constrained with pins or clamps. The model should retain the dynamic characteristics of the larger steam dryer model, such as having closely spaced natural frequencies. The analysis should include the following aspects:

(a) One percent Rayleigh damping would be used for the transient simulations. Estimate the actual damping value at each natural frequency of the simplified model (i.e., small section of dryer) and use them in performing new frequency based simulations. Stress and displacement time histories at high stress locations from both approaches would be compared [[

]]. Maximum stresses and displacements for both approaches would then be compared at several locations on the hood.

(b) Along with comparing time series computed using the transient and frequency based simulations for a model like the one described in part (a), PSEG should provide comparisons of Fast Fourier Transforms, as specified in the original RAI, and explain any differences between peak levels.

(c) Reevaluate the frequency simulations considered in Part (a) of this RAI with 1 percent of the critical damping for all the frequencies and the compare the results for high stresses, displacements and alternating stress ratios with those for the transient simulations presented in Part (a). Provide justification for the differences in the results.

Response

A comparison between the harmonic and time-domain methods is performed in Appendix B of CDI Report 07-17P at two frequencies (15 Hz and 120 Hz). There, the applied load is the acoustic pressure field at the respective frequencies obtained by solving the Helmholtz equation in the steam dome. Therefore the examples retained complexity in both the structural model (the full steam dryer was considered) and the

spatial distribution of the applied load. However, the variation of the load in time was a simple sinusoid and one objective of the RAI is to establish agreement between the time-domain and harmonic approaches for a complicated time varying loading. It is recognized that the underlying theory of the harmonic and time domain approach is not in question, i.e., the mathematical soundness of the approach and theoretical agreement (at infinite spatial and temporal resolution, etc.) between the two approaches is accepted. Instead, the verification focuses on the implementation of the harmonic method and requests demonstration that the software embodiment of the harmonic method shows good agreement with time-domain solutions.

The second objective is to evaluate the effect of using two different damping models, specifically a Rayleigh damping model and one that enforces 1% critical damping at all frequencies. Unless a complete modal decomposition is performed, then the time domain method can only employ the Rayleigh damping model where 1% damping is enforced at two 'pin' frequencies. Between these frequencies the damping is less than specified (and therefore overly conservative); elsewhere the damping is higher. The harmonic method can enforce 1% damping over the entire frequency range.

The main challenge in comparing the time-domain and harmonic responses for a complete steam dryer over the typical 0-200 Hz frequency range is the time required to perform the time-domain calculation. The costs are discussed in Appendix B and amount to multiple weeks of parallel computing time, terabytes of storage and susceptibility to power interruption. These computational costs motivated a modified approach that retains complexity for the applied loading in both space and time.

With this approach, the complete steam dryer is considered and subjected to an acoustic forcing that is complex in both space and time, but limited to a frequency range of 100 Hz to 150 Hz. Limiting the frequency range reduces the computation time which scales in proportion to f_{max}/f_{min} where f_{min} and f_{max} are the smallest and highest frequencies considered in the calculation. In production steam dryer calculations f_{min}=10 Hz and f_{max}=200 Hz. Limiting the frequency range to f_{min}=100 Hz and f_{max}=150 Hz reduces computation time 13-fold yet retains all of the complexities inherent in production runs. The one drawback with this option is that since the transient simulation is started from rest, lower frequency modes (i.e., less than 100 Hz) are also excited and their associated transients not fully damped by the end of the calculation. This behavior is evident, for example, in the 120 Hz simulation in Appendix B of CDI Report 07-17P which shows the presence of a small transient for a mode whose characteristic frequency is less than 120 Hz.

The following four calculations were set up and executed:

(i) Harmonic calculation with 1% damping enforced at all frequencies. This calculation was done earlier for CDI Report 07-17

(ii) Harmonic calculation with a Rayleigh damping model with 1% damping enforced at the pin frequencies of 10 Hz and 150 Hz;
(iii) Transient calculation starting from rest with the same Rayleigh damping model; and
(iv) Transient calculation started with initial conditions obtained from the harmonic calculation with Rayleigh damping. This last calculation resulted after further consideration on how to reduce calculation times in the transient method, as discussed below.

In all four calculations, the forcing is the same as used in CDI Report 07-17 for CLTP conditions, but retaining only those frequency components in the range 100 Hz to 150 Hz. In the transient calculation, the acoustic pressure field at any time step is obtained by summing the Fourier components of the acoustic field over the 100-150 Hz frequency range. The Rayleigh damping model is the same as used in previous transient simulations for the Hope Creek steam dryer (CDI Report 06-27, Rev. 2) and also produces significant variation in the effective damping ratio over the frequency range considered here (0.72% at 100 Hz to 1% at 150 Hz).

For the transient simulations the step size is chosen as 0.0002 seconds which resolves the 150 Hz frequency component at 33.3 steps per cycle. This is higher than the 20 steps per cycle recommended by ANSYS. The simulation time interval was initially set to 1 second. [[

[[(3)]]

Evaluations are made by comparing the time histories predicted by each calculation method. In all calculations, the stress component σ_{xx} is computed at every location below on one of the adjacent plates. The following measures of response amplitude and error are useful for quantitative comparison. Denoting the stress history obtained at a node using calculation, m, by $\sigma_m(t)$, then define:

$$\sigma_m^{max} = \max\{|\sigma_m(t)|\}$$

$$\sigma_m^{alt} = \frac{1}{2}\left(\max\{\sigma_m(t)\} - \min\{\sigma_m(t)\}\right)$$

$$e_{m,n}^{max} = \frac{\sigma_m^{max} - \sigma_n^{max}}{\max\left\{\sigma_m^{max}, \sigma_n^{max}\right\}}$$

$$e_{m,n}^{alt} = \frac{\sigma_m^{alt} - \sigma_n^{alt}}{\max\left\{\sigma_m^{alt}, \sigma_n^{alt}\right\}}$$

Briefly, σ^{max} is a measure of the maximum stress experienced during the response and σ^{alt} measures the difference between the minimum and maximum stresses during the response and thus is representative of an alternating stress. The error, $e_{m,n}^{max}$, represents

the difference in σ^{max} obtained by methods m and n, normalized by σ^{max}. $e^{alt}_{m,n}$ represents a similar error measure for the alternating stress.

The stress responses are compared at nodes selected from Table 7b of CDI Report 07-17P. These nodes exhibited the strongest alternating stress intensities or maximum stress intensities at one of the frequency shifts. As shown in that report, the response was dominated by a strong 80 Hz signal that is not included in the frequency range being considered here. As a result, the stresses calculated here tend to be smaller at these nodes. However, this has no bearing upon the conclusions reached here. In particular, the excellent agreement demonstrated here between harmonic and transient solutions using the same damping models is expected to hold over other frequency ranges. When comparing different damping models, one expects that the differences would be even higher than shown here if the 80 Hz frequency was included in the frequency range. This is because the effective damping ratio at 80 Hz using Rayleigh damping (0.62%) is lower than the smallest value (0.72%) in the 100-150 Hz frequency range. For the same reasons one would expect transient overshoots to be higher at the 80 Hz frequency though it is difficult to quantify exactly by how much.

In the following discussion, emphasis is placed on stress results. Generally matching stresses poses a more stringent test than comparing displacements since stresses are derivative quantities and thus more strongly affected by discretization error. Furthermore, while stresses are of direct concern in steam dryer analysis, displacements are normally of lesser significance.

Effects of Damping

The influence of the damping model on the computed stresses is assessed by comparing the harmonic responses at selected nodes. Specifically the calculations (i) and (ii) described above are compared. The Rayleigh damping varies from 0.72% to 1%, one expects, that the stress peaks obtained with the Rayleigh model will be between 0% to 39% higher than when using a 1% damping at all frequencies. The stress and error measures defined above are recorded at the selected nodes in Table14.110. 1. The responses are compared in Figure 14.110.1. The main observation is that the predicted maximum and alternating stresses obtained with the Rayleigh damping model are everywhere higher than those obtained with 1% damping model. This is entirely consistent with expectations. The differences at these sample locations are up to 11%. Higher differences can be expected at other locations particularly ones where the local response is dominated by a mode with natural frequency near 100 Hz. Another interesting observation is that even where stresses are very small (e.g., node 88325) the responses agree to within 9.3% error. Hence, as expected, the use of different damping models tends to scale the response rather than to introduce an additive error.

Node	σ_1^{max} (psi)	σ_2^{max} (psi)	σ_1^{alt} (psi)	σ_2^{alt} (psi)	$e_{1,2}^{max}$ (%)	$e_{1,2}^{alt}$ (%)
82290	27.16	30.45	27.03	30.38	-10.8%	-11%
86424	5.827	6.096	5.672	5.988	-4.4%	-5.3%
82652	8.260	8.868	8.215	8.833	-6.9%	-7%
88325	$6.1\ 10^{-4}$	$6.72\ 10^{-4}$	$5.93\ 10^{-4}$	$6.54\ 10^{-4}$	-9.2%	-9.3%
88252	23.32	23.46	23.1	23.19	-0.6%	-0.4%

Table 14.110.1 Maximum stresses and stress errors resulting from different damping models.

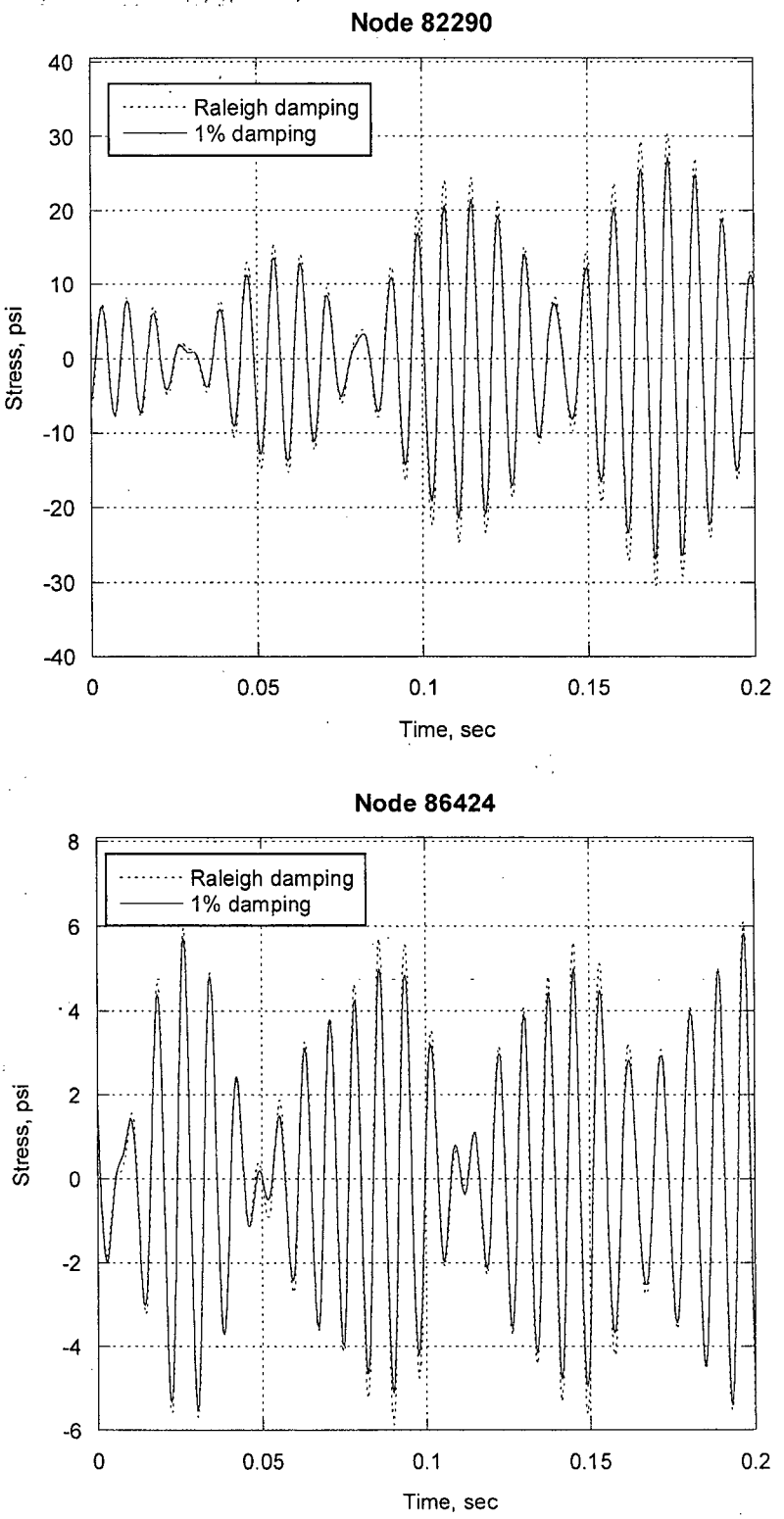

Figure 14.110.1a. Comparison of harmonic solutions with Raleigh damping and flat 1% of critical damping. Dashed red line – Rayleigh damping. Solid blue line – 1% flat damping. Nodes 82290 and 86424.

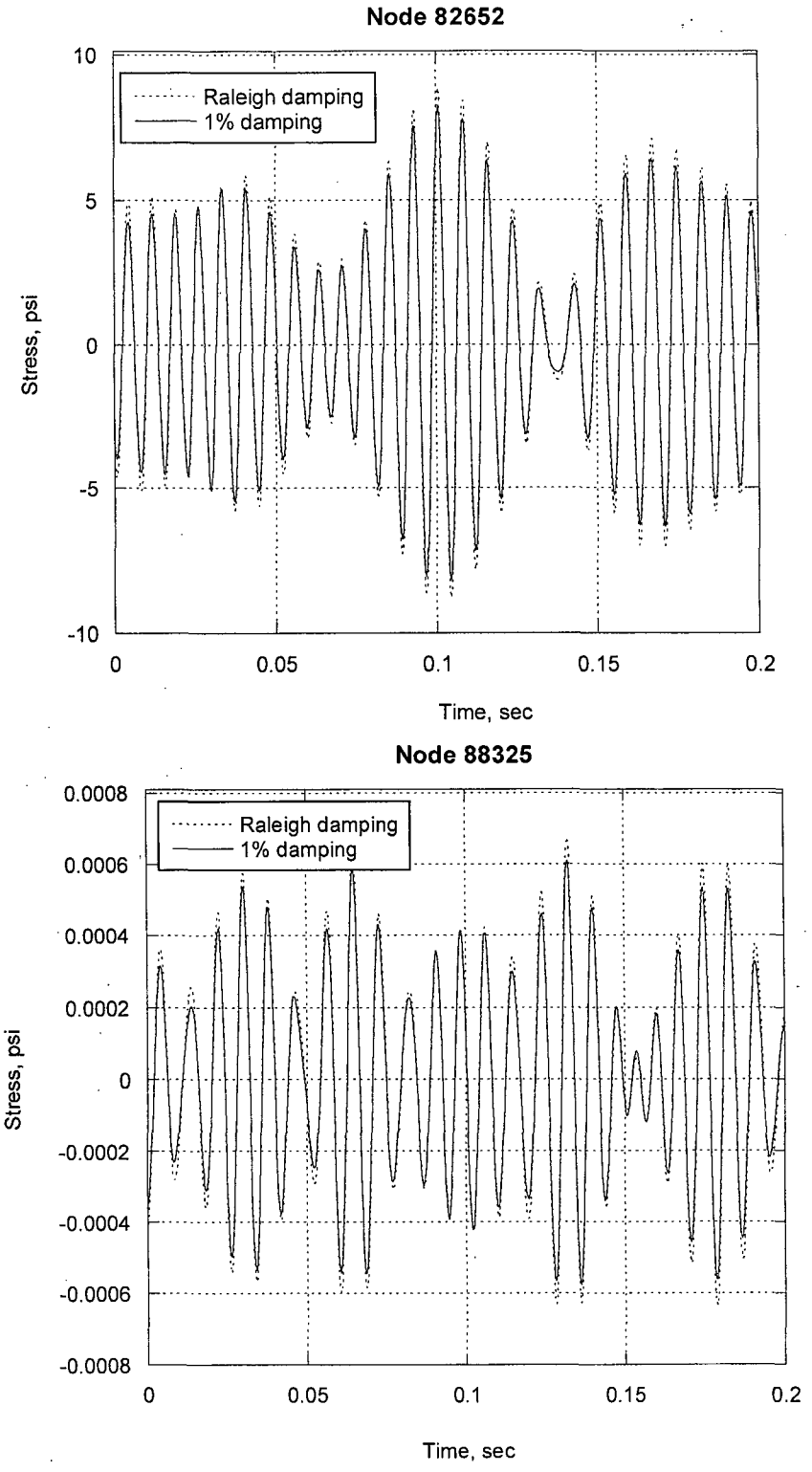

Figure 14.110.1b. Comparison of harmonic solutions with Raleigh damping and flat 1% of critical damping. Dashed red line – Rayleigh damping. Solid blue line – 1% flat damping. Nodes 82652 and 88325.

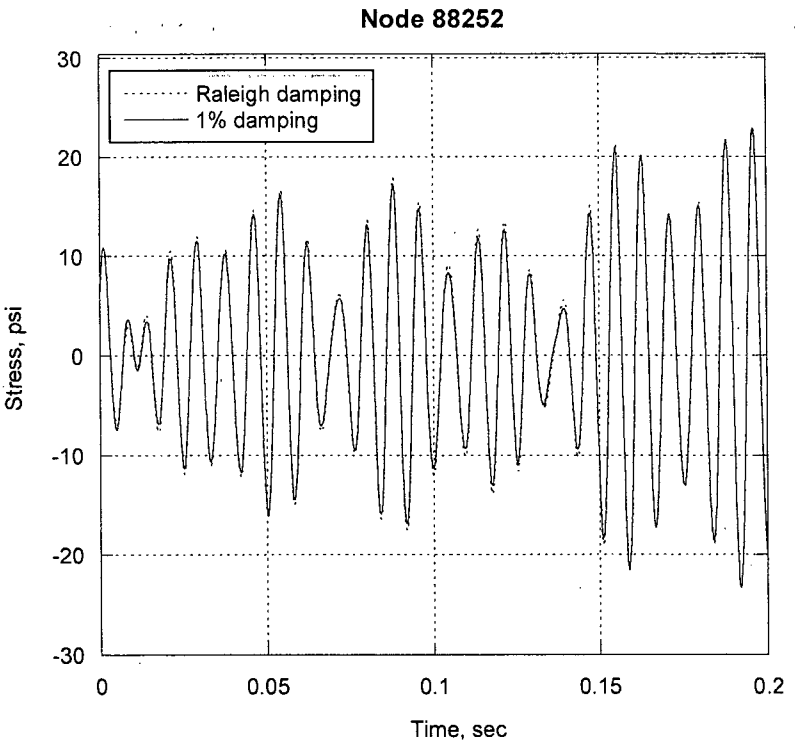

Figure 14.110.1c. Comparison of harmonic solutions with Raleigh damping and flat 1% of critical damping. Dashed red line – Rayleigh damping. Solid blue line – 1% flat damping. Node 88252.

Comparison of Harmonic and Time-Domain Predictions of Steady State Stresses
The next comparison examines the responses obtained with the same damping model (Rayleigh damping), but using different prediction methods – the transient or time marching approach and the harmonic analysis. In the transient analysis, the initial conditions (displacements and velocities) are set from the harmonic analysis results in order to minimize the presence of transients in the response. Mathematically, identical responses are expected and the goal here is to verify whether this is reflected in the computational implementation. The results are tabulated in Table 14.110.2 and depicted in Figure14.110.2. As expected very good agreement is established overall. In all figures, the agreement is demonstrated in both phase and amplitude and, with the exception of node 86424, the response curves are virtually indistinguishable. For node 86424 (Figure 14.110.2b), the maximum error occurs towards the end of the simulation. The difference in results for this node can be attributed to:

(i) temporal discretization errors – the transient time integration algorithm is second order accurate and thus has errors proportional to Δt^2;
(ii) frequency discretization errors – the frequency schedule is selected to ensure a worst case error of 5% in the response peak amplitude. This frequency schedule presumes 1% damping. Since the Rayleigh damping implies lower damping ratios in the current case (down to 0.72% damping) the worst case error is correspondingly higher (up to 5%/0.72 = 6.9%). The average error is considerably less.
(iii) initial condition errors – the initial conditions are also calculated to within the discretization accuracy afforded by the frequency domain calculation.

Note too that the difference between the harmonic and transient responses for node 86424 varies periodically, peaking every seven cycles or so. This is consistent with initial condition error or, possibly, excitation of a lower frequency mode in startup. For all other nodes, errors are less than 3% which is within the maximum error bound (6.9%) given theoretically.

Table 14.110.2. Comparison of harmonic and transient calculations. Index 1 corresponds to harmonic solution, index 4 corresponds to transient calculation with adjusted initial conditions.

Node	σ_2^{max} (psi)	σ_4^{max} (psi)	σ_2^{alt} (psi)	σ_4^{alt} (psi)	$e_{2,4}^{max}$ (%)	$e_{2,4}^{alt}$ (%)
82290	30.45	29.58	30.38	29.58	2.9%	2.6%
86424	6.096	6.667	5.988	6.333	-8.5%	-5.5%
82652	8.868	8.647	8.833	8.643	2.5%	2.2%
88325	$6.72\ 10^{-4}$	$6.51\ 10^{-4}$	$6.54\ 10^{-4}$	$6.37\ 10^{-4}$	3.1%	2.6%
88252	23.46	23.12	23.19	22.85	1.5%	1.5%

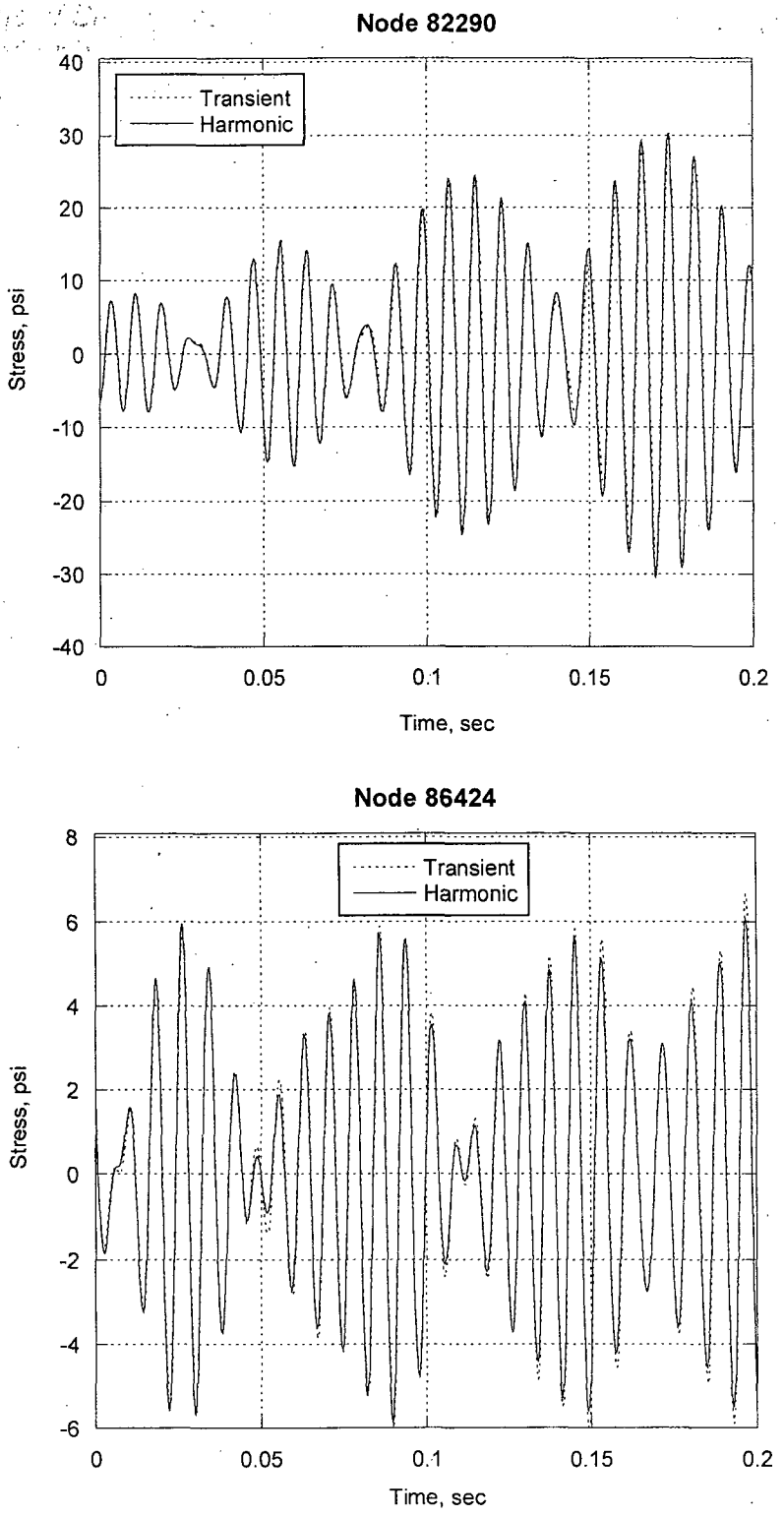

Figure 14.110.2a. Comparison of harmonic and transient solution with adjusted initial conditions. Dashed red line – transient; solid blue line – harmonic. Nodes 82290 and 86424.

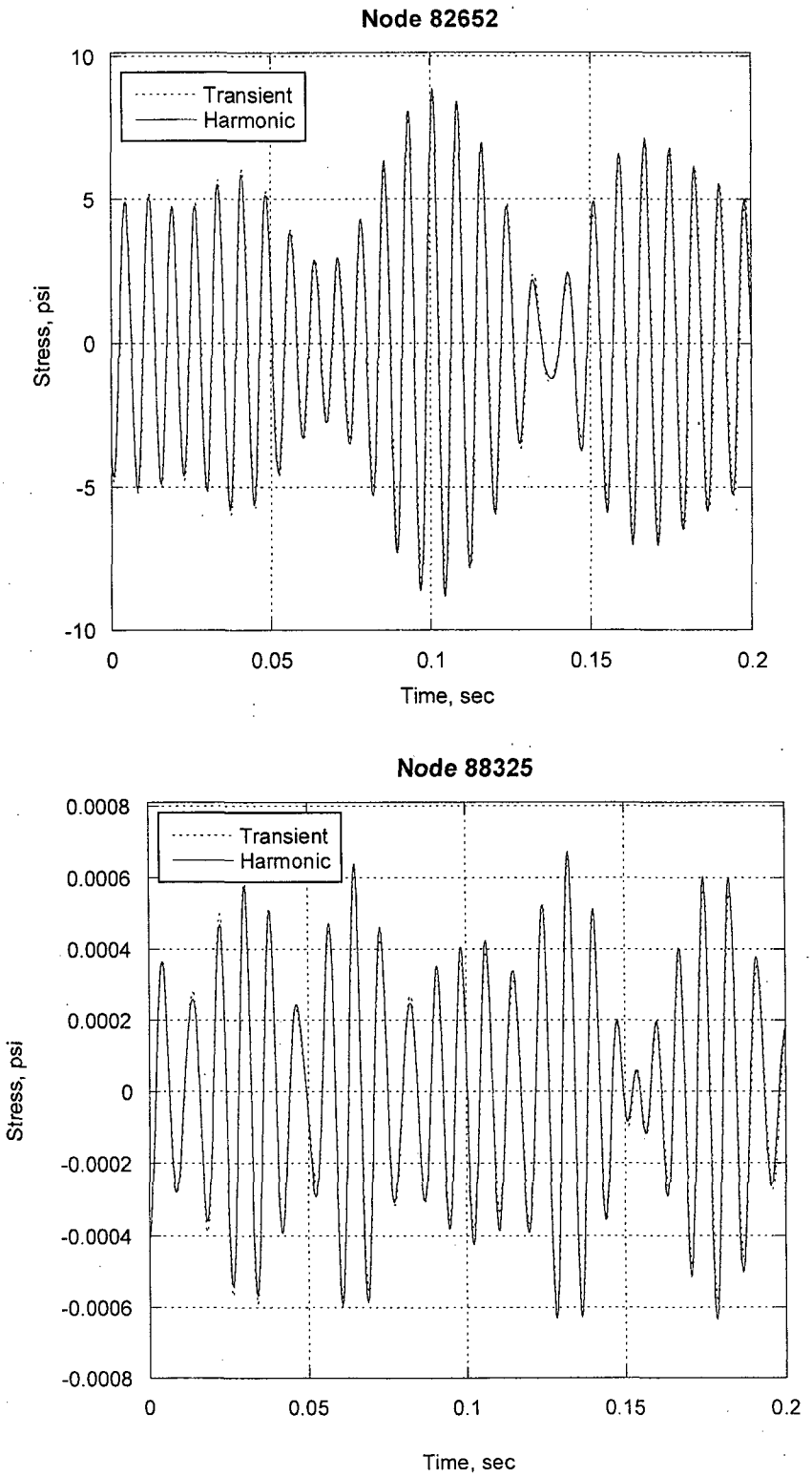

Figure 14.110.2b. Comparison of harmonic and transient solution with adjusted initial conditions. Dashed red line – transient, solid blue line – harmonic. Nodes 82652 and 88325.

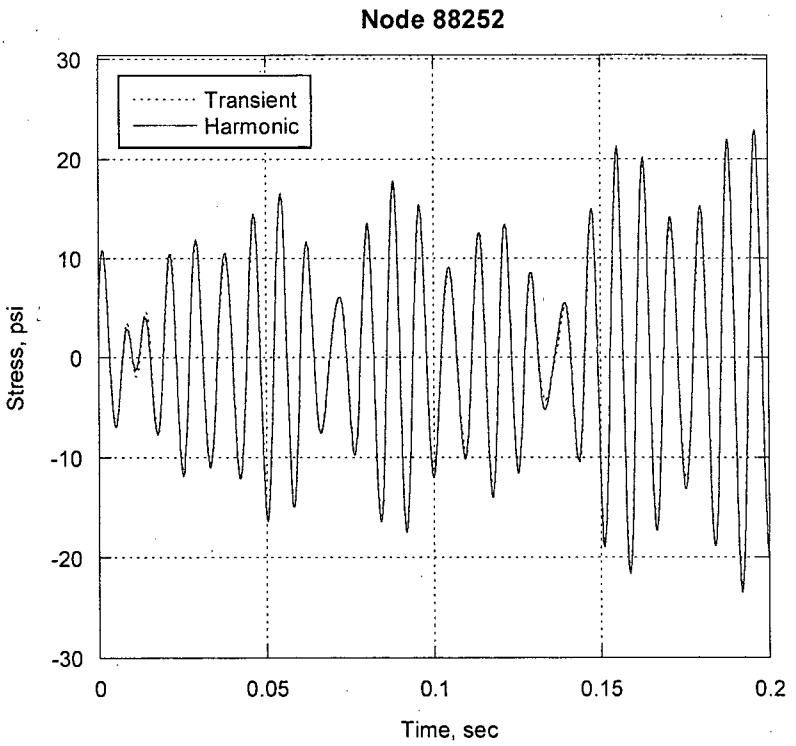

Figure 14.110.2c. Comparison of harmonic and transient solution with adjusted initial conditions. Dashed red line – transient; solid blue line – harmonic. Node 88252.

[[

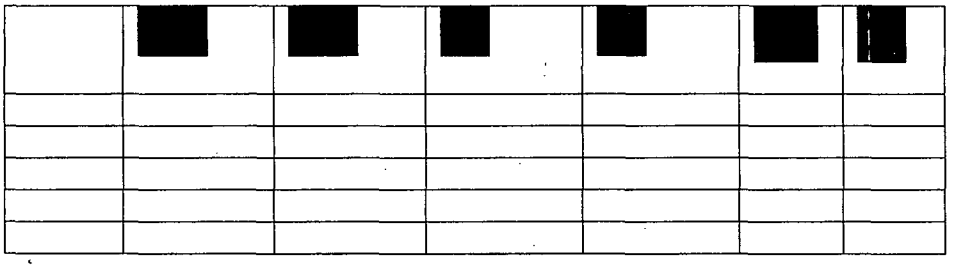

[3]]]

[[

]]^(3)

Figure 14.110.3a. Comparison of transient calculations with zero initial conditions (IC) and initial conditions calculated from harmonic solution. Solid blue line – zero IC; dashed red line – adjusted (or non-zero) IC. Nodes 82290 and 86424.

[[

]]$^{(3)}$

Figure 14.110.3b. Comparison of transient calculations with zero initial conditions (IC) and initial conditions calculated from harmonic solution. Solid blue line – zero IC; dashed red line – adjusted (or non-zero) IC. Nodes 82652 and 88325.

[[

(3)]]

Figure 14.110.3c. Comparison of transient calculations with zero initial conditions (IC) and initial conditions calculated from harmonic solution. Solid blue line – zero IC; dashed red line – adjusted (or non-zero) IC. Node 88252.

PSD comparison

The power spectral density (PSD) of stress component σ_{xx} is calculated for two of the nodes, 82290 and 88252. Since the estimate was calculated from 0.2 sec time histories the frequency resolution is only 5 Hz. The comparison in the frequency range from 100 Hz to 150 Hz is shown in Figure 14.110.4 for node 82290 and in Figure 14.110.5 for node 88252.

The effect of damping (Figures 14.110.4a and 14.110.5a) is similar to that observed above in the stress time histories, i.e., the PSD corresponding to the Rayleigh damping model is generally larger since the effective damping in this frequency range is smaller. From Figure 14.110.4a, the effect is seen to be frequency dependent. When using the same damping models the PSDs extracted from the harmonic and time-marching calculations (the latter being started with transient-free initial conditions) are in excellent agreement (Figures 14.110.4b and 14.110.5b). The small mismatches (recall that these results are plotted on logarithmic scales) near 100 Hz and 150 Hz are due, in part, to leakage into neighboring bins when computing the PSD. Finally, the PSDs obtained from the transient simulations initiated with the transient free solutions and with zero initial conditions are compared in Figures 14.110.4c and 14.110.5c. These plots

indicate that the presence of start up transients over this time interval can result in both under- and over-predictions of stresses.

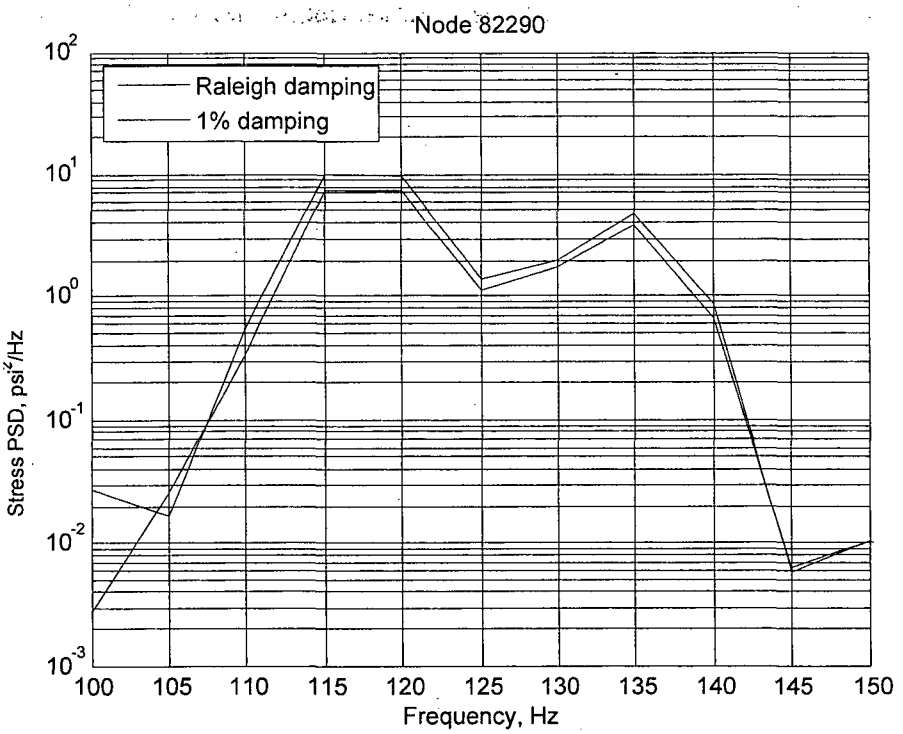

Figure 14.110.4a. PSD comparison of the harmonic solutions obtained with Rayleigh damping and constant 1% critical damping. Dashed red line – Rayleigh damping. Solid blue line – 1% flat damping. Node 82290.

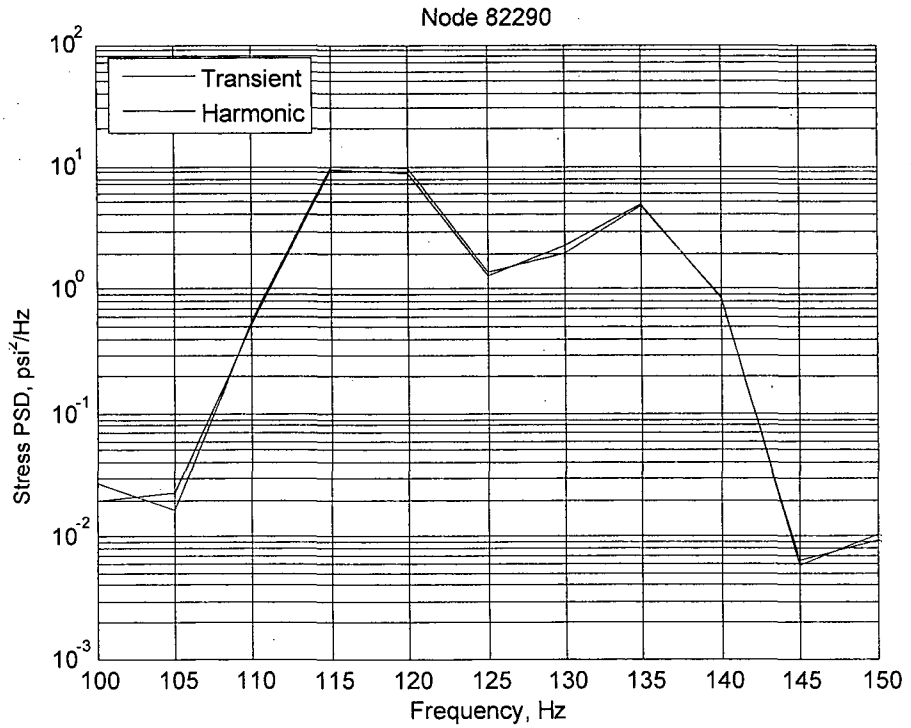

Figure 14.110.4b. Comparison of harmonic and transient solution with adjusted initial conditions. Dashed red line – transient, solid blue line – harmonic. Node 82290.

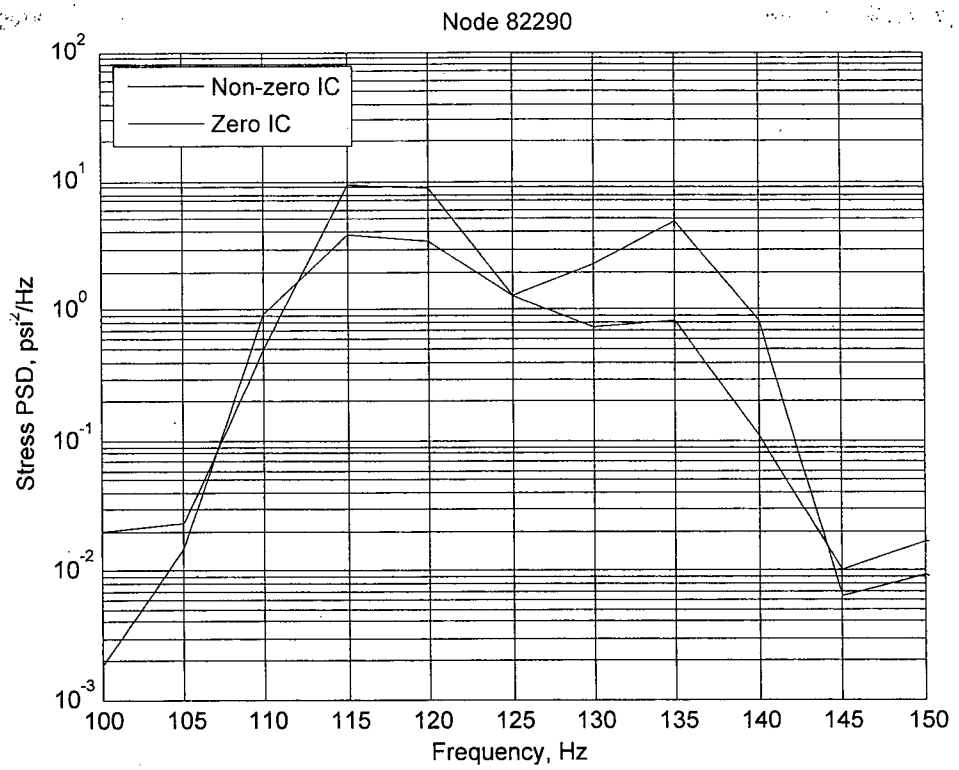

Figure 14.110.4c. Comparison of transient calculations with zero initial conditions (IC) and initial conditions calculated from harmonic solution. Solid blue line – zero IC; dashed red line – adjusted (or non-zero) IC. Node 82290.

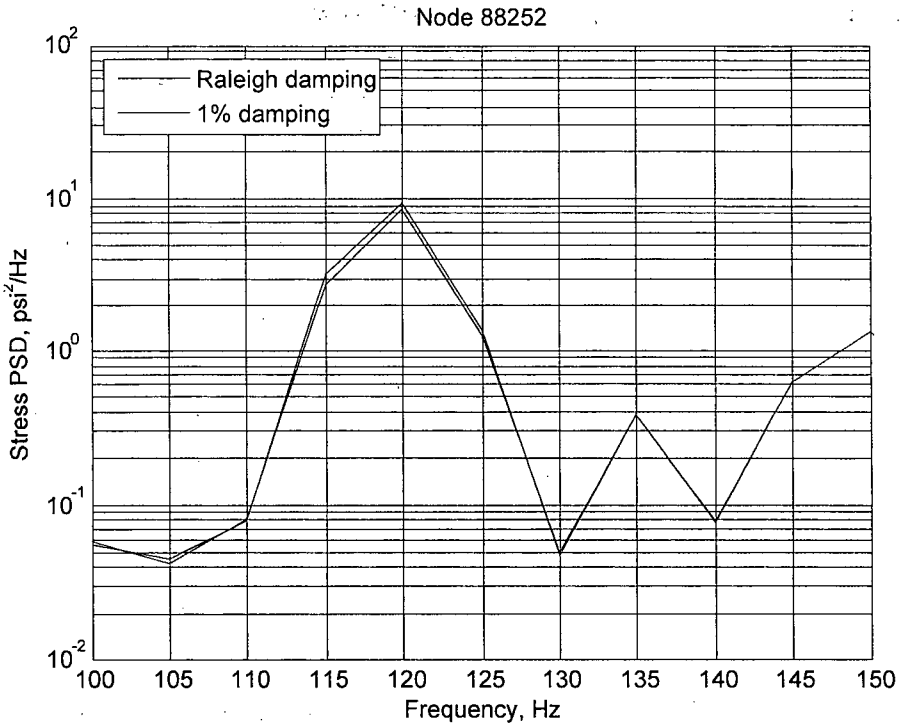

Figure 14.110.5a. PSD comparison of the harmonic solutions obtained with Rayleigh damping and constant 1% of critical damping. Dashed red line – Rayleigh damping. Solid blue line – 1% flat damping. Node 88252.

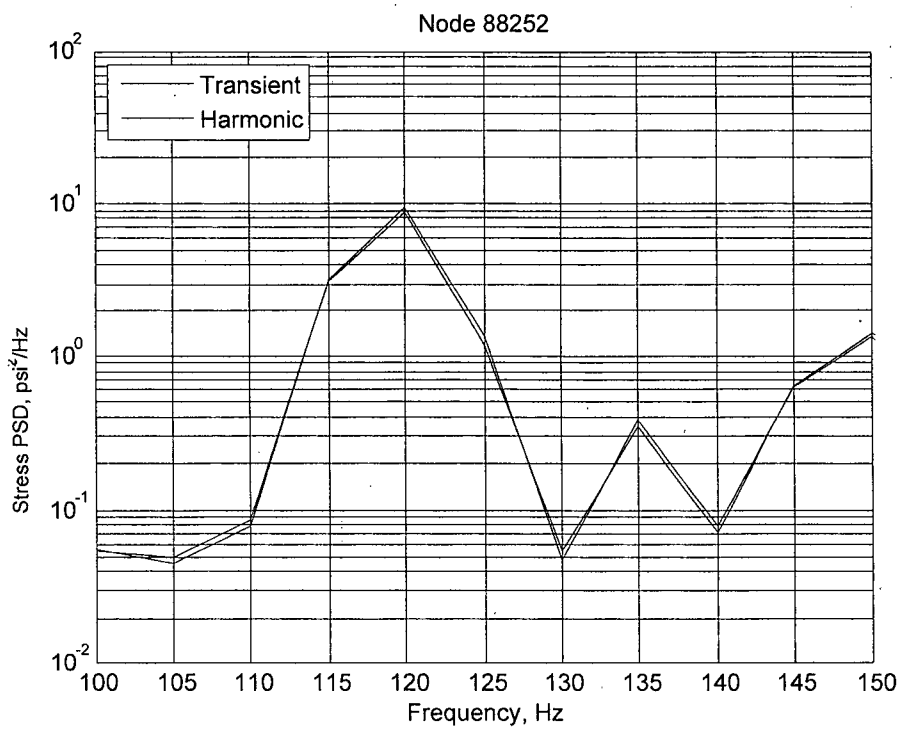

Figure 14.110.5b. Comparison of harmonic and transient solution with adjusted initial conditions. Dashed red line – transient, solid blue line – harmonic. Node 88252.

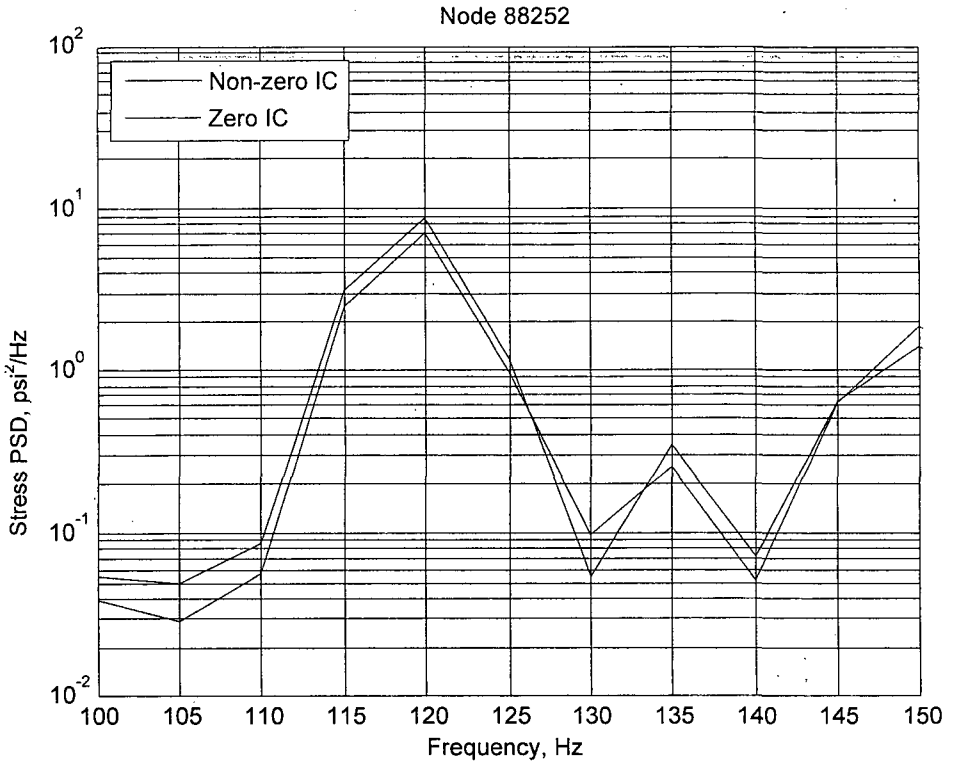

Figure 14.110.5c. Comparison of transient calculations with zero initial conditions (IC) and initial conditions calculated from harmonic solution. Solid blue line – zero IC; dashed red line – adjusted (or non-zero) IC. Node 88252.

Summary

The comparisons carried out above have shown that:

(i) Excellent agreement is achieved when comparing the harmonic and transient responses obtained for identical steam dryer models and damping models. This agreement is demonstrated for a load that is complex in both space and time and is established for both amplitude and phase. Remaining discrepancies can be attributed to discretization error in the time integration scheme and/or frequency schedule discretization.

(ii) The effects of damping (Rayleigh vs. constant 1% damping) upon the periodic response behave as expected. In this case the Rayleigh damping model results in overpredictions of the stress response due to lower effective damping.

(iii) [[

$^{(3)}$]]

Additional RAI 14.111

[[

]]. PSEG is requested to explain why such large differences exist in the source strengths.

Response
[[

[3]]] So some asymmetry is to be expected.

[[

[3]]]

Figure RAI14.111.1. [[
[3]]] The colors indicate the main steam line data plotted (Figure 4.1 of C.D.I. Report No. 07-09P).

[[

]]

Figure RAI14.111.2. [[ ]]

Additional RAI 14.112

[[

]]. PSEG is requested to provide this report for evaluation of the new methodology.

Response
C.D.I. Report No. 04-09P is provided in Attachment 3.

Additional RAI 14.113

In CDI Report No. 07-09P, a new ACM Rev. 4 is developed to improve prediction of the dryer load at low frequencies. [[

]]

Response
[[

[[ ]](3)]]

Additional RAI 14.114

In the development of the hydrodynamic load contribution on page 8 of CDI Report No. 07-09P, reference is made to pressure fluctuations $p = 0.1 \rho U^2$. It is not clear whether this estimate is used in equation 4.1 for the [[ ]]. The other parameters used in equation 4.1 are also not clear. PSEG is requested to:

(a) if the estimate $p = 0.1 \rho U^2$ is used in equation 4.1, validate this estimate from [[ ]] on the dryer, e.g. from QC2 dryer measurements; and

(b) [[ ]]

Response

(a) The estimate $p = 0.1 \rho U^2$ is not used for the source strength. It results from estimating the pressure fluctuations from turbulent buffeting from $q=1/2\rho U^2$ and assuming that U is the steady flow velocity and the velocity fluctuations are 10% of the steady flow velocity.

[[ ]](3)]]

(b) Equation 4.1 is:

$$\Delta P = K\frac{\rho}{2}\frac{U^2}{\eta_o^2}\left\{2\frac{u'}{U} - \frac{2\eta'}{\eta_o}\right\}$$

with the following variables:

(1) The variable K/η_o^2 is the pressure loss coefficient associated with the inlet to the main steam and has the value of 1.0 in the ACM model.

(2) The variable η'/η_o is the normalized unsteady fluctuation in the vena contracta and is a dependent variable in the ACM model. [[

[3]]]

(3) The variable u'/U is the normalized velocity fluctuation into the main steam line and is also a dependent variable in the model that is directly determined from the two independent pressure measurements made on each steam line. Again, no value can be prescribed for u' since it is a dependent variable. In Report No 07-09P the subscript lower case b is a typographical error and should be dropped so that $\acute{u}_b = u'$.

Additional RAI 14.115

On page 4 of CDI Report No. 07-09P, CDI develops a new ACM code to improve the prediction of dryer load at low frequency. The report states that the Helmholtz and Acoustic Circuit Model (ACM) analyses are driven by [[ ]]. In the new ACM Rev. 4, it appears that [[

]]. PSEG is requested to provide the

[[

]].

Response
The ACM modeling parameters are summarized below:
[[

[(3)]]

Additional RAI 14.116

The pressure fluctuations measured by the strain gages on the MSLs contain noise signals that are not acoustic in nature. In CDI Report No. 07-09P, the [[

]]. In particular, PSEG should provide:

(a) [[ ]];

(b) [[

]]; and

(c) more detailed explanation of step 3.

Response

As discussed in C.D.I. Report No. 07-09P, signal noise is removed from the data by three means:

(a) [[

[[(3)]]

(b) [[

[[(3)]]

(c) [[

[[(3)]]

Additional RAI 14.117

Referring to CDI Report No. 07-09P, the predictions of ACM Rev. [[

]]. PSEG is requested to explain [[

]].

Response
The 60 to 70 Hz underestimate is combined with the 70 to 100 Hz overestimate to produce the bias and uncertainty in the frequency range 60 to 100 Hz. These intervals are consistent with that used in the Rev. 2 model, and are: 0-20, 20-40, 40-60, 60-100, 100-150, 150-200, 200-250, and 116-120 (around the peak frequency).

The intervals can always be redefined, and a decision was made to use the same intervals in the Rev. 4 model that were used in the Rev. 2 model, which we believe were acceptable. [[

(3)]]

[[

[3]]]

PSD of the maximum pressure loads predicted on the C-D side of the HC1 dryer (top) and A-B side of the NC dryer (bottom).

Additional RAI 14.118

Benchmarking of the new ACM Rev. 4 against the data of QC2 dryer is presented in CDI Report No. 07-09. PSEG has not demonstrated that this benchmarking is an adequate validation of the new methodology. For example, the low frequency loading on the dryer of QC2 is relatively small, and the [[
]]. The new version of ACM Rev. 4 needs to be validated against data from additional dryers exposed to strong low frequency loading. PSEG is requested to provide validation of this new methodology against additional dryer data.

Response
No additional data sets are available to PSEG to undertake further validation of ACM Rev. 4. Comparison of prediction against the Quad Cities data is favorable. [[

[3]]]

Examining steam line data between Quad Cities and Hope Creek (see for instance MSL C upper location on Figure RAI14.118.1) the low frequency pressures are greater on Quad Cities than on Hope Creek's main steam line above 15 Hz.

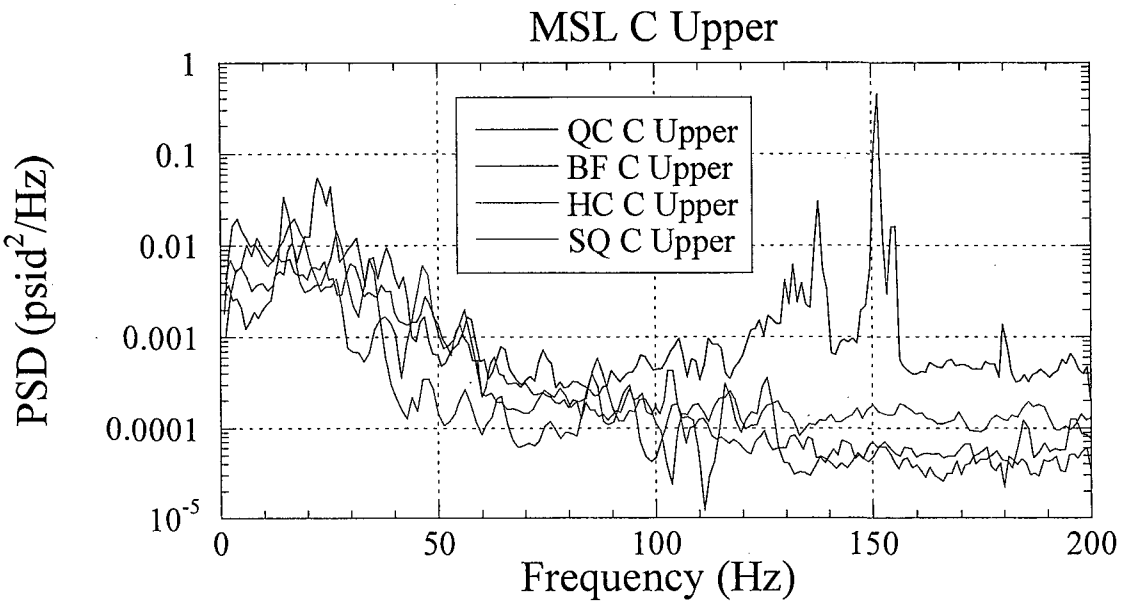

Figure RAI14.118.1: Comparison of Quad Cities (QC), Browns Ferry (BF), Hope Creek (HC),and Susquehanna (SQ) main steam line data.

Additional RAI 14.119

In CDI Report no. 07-18, ACM Rev. 4 is used to predict the dryer load of HC1 from strain gage measurements on MSLs. No details however are given regarding the [[ ]]. PSEG is requested to provide the following:

(a) [[

]].

(b) [[

]].

(c) [[

]].

(d) [[

]].

Response

(a) The PSDs are shown in Figure RAI14.119.1. *
(b) The dipole orientation is described in response to RAI 14.113.
(c) The ACM model parameters are summarized in response to RAI 14.115.
(d) The parameters are described in response to RAI 14.114.

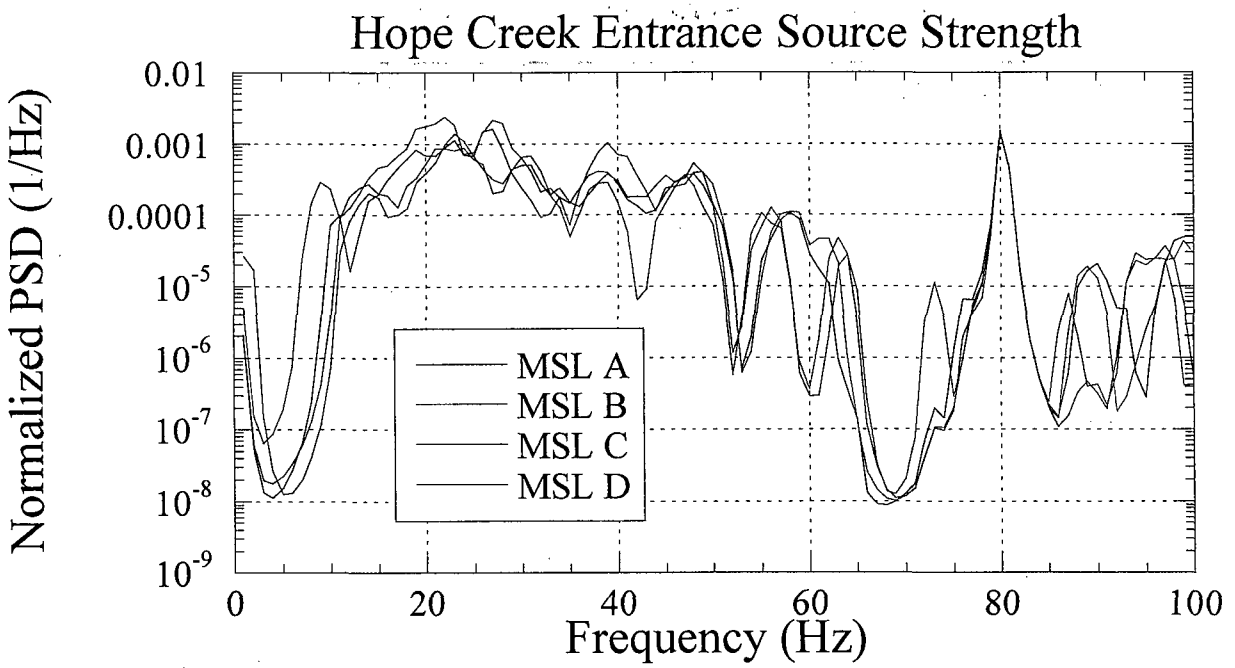

Figure RAI 14.119.1: Normalized PSD of entrance source strengths η' for Hope Creek CLTP conditions. The colors indicate the main steam line data plotted. Note that the 80 Hz peak has been retained.

*Note that below 10Hz these dipole source strengths are lower than those at Quad Cities. However one should not necessary conclude that the low frequency loads will be lower as well since the low frequency loads result form both a monopole and dipole source.

Additional RAI 14.120

In CDI Report No. 07-18P, the [[

]] In CDI Report No. 07-17P, 90 percent of this signal is filtered out based on the determination that this component is not present in the pressure measurements taken from the steam dome (see page 79 of CDI Report No. 07-17P). However, the absence of the [[

]]. Although consideration of the full strength of the [[

]] (i.e. still results in a positive stress ratio), PSEG is requested to provide additional information to [[

]].

Response

[[

[[(3)]]

[[

(3)]]

Figure 14.120-1a: PSDs of the pressure signals for main steam line A.

[[

(3)]]

Figure 14.120-1b: PSDs of the pressure signals for main steam line B.

[[

(3)]]

Figure 14.120-1c: PSDs of the pressure signals for main steam line C.

[[

(3)]]

Figure 14.120-1d: PSDs of the pressure signals for main steam lines D.

Note that the filtering applied to the CLTP data is based on coherence. The coherence for these four lines in the 70-90 Hz frequency range is shown on Figure 14.120-3. It can be seen that the coherence values are of the order of 0.3 or less. It is anticipated that if the pressure fluctuations between the strain gauges were the result of acoustic waves, the coherence values would approach 1.0. In this frequency range the signal is noise. Furthermore once coherence values fall below 0.15, the signal is set equal to zero,

which cannot be plotted on a logarithmic scale. See CDI report 07-18P for the filter algorithm.

[[

(3)]]

Figure 14.120-2: Pressure load comparison at outer bank hood with 0.25 Hz frequency increments

[[

(3)]]

Figure 14.120-3 Coherence of MSL signals between 70 and 90 Hz at CLTP condition.

Additional RAI 14.121

The following questions are intended for clarification of CDI Report 07-17P:

(a) In Equation (6), why is the right-hand side multiplied by $(1 + \lambda)$?

Response
The multiplication by the factor $(1+\lambda)$ where λ is the frequency shift follows directly from the properties of Fourier transforms (e.g., scaling properties in Press, W.H., Teukolsky, S.A., et al, Numerical Recipes in Fortran, 2nd Edition, Cambridge University Press, 1992, pg. 491) which states that for the transform pair $h(t) \Leftrightarrow H(f)$:

$$h(at) \Leftrightarrow \frac{1}{a} H(f/a)$$

Setting $a=1/(1+\lambda)$ proves the result. Note that what is actually done in 'frequency shifting' is to stretch or compress the function in the time domain (i.e., $h(t) \rightarrow h(at)$) with amplitudes preserved. In the frequency domain this is equivalent to scaling the frequencies and amplitudes as indicated.

(b) In Section 2.3, first paragraph, it is stated, "Off-surface loads are required by ANSYS to ensure proper interpolation of forces." What are off-surface loads? Please explain the statement.

Response
Physically, the acoustic pressure field is applied to the steam dryer surface. Thus at a given point on the surface, $\mathbf{R}_s$, the applied stress is $-P(\mathbf{R}_s)\mathbf{n}_s(R_s)$, where $P(\mathbf{R}_s)$ is the acoustic pressure evaluated at $\mathbf{R}_s$ and $\mathbf{n}(\mathbf{R}_s)$ is the local normal directed into the fluid. In order to impose this load numerically, ANSYS employs load tables where the pressures forces are represented on a $n_x \times n_y \times n_z$ regular lattice. In general the lattice points do not line up exactly with the surface. However, the lattice spacing is made sufficiently small (3 inches) to accurately resolve the spatial variations of the acoustic field. For any surface points, $\mathbf{R}_s$, the surface pressure force is obtained by first identifying the cube-shaped lattice cell containing the point. This cell will have 8 forming corners or vertices which contain the acoustic pressures. These points are strictly off the surface (hence their name)– some being slightly above the surface and others slightly below. However, all vertices are within 3 inches of $\mathbf{R}_s$ and $P(\mathbf{R}_s)$ is obtained by linearly interpolating the vertex values.

(c) In Section 2.3, second paragraph, first sentence states, [[
]] Please explain this sentence. The last sentence of this paragraph states, "Linear interpolation is sufficient since the

pressure load varies slowly over [[ ]] Please explain why the [[
]].

Response
[[

[3]]]

The structural responses to these solutions vary more rapidly with frequency, however. Thus, while the load may be accurately interpolated by linear interpolation over a 5 Hz interval, the structural response can not be accurately interpolated in the same way. To accurately interpolate the structural response the frequency spacing must be sufficiently dense to resolve the resonant peaks. The required spacing is directly controlled by the structural damping (which effectively smears out the resonant peaks) and numerical experiments have shown that for 1% damping a spacing $\Delta f=f/157$ will resolve the peaks to within 5% of their maximum values.

To illustrate, consider a single degree of freedom spring-mass-damper system:

$$\ddot{x} + 2\zeta\omega_n\dot{x} + \omega_n^2 x = F(\omega)e^{i\omega t}$$

where x is the displacement, ζ is the damping ratio, ω_n is the natural frequency, ω is the circular frequency and $F(\omega)$ is a slowly varying force amplitude. Suppose that the force amplitude can be adequately represented between frequencies, ω_1 and ω_2, by the linear function:

$$F(\omega) = F_1 + (F_2 - F_1)\frac{f - f_1}{f_2 - f_1}$$

where $f=\omega/2\pi$ is the frequency. Then the well-known harmonic response amplitude, $X=|x|$ is:

$$X(\omega) = \frac{F(\omega)}{\sqrt{(\omega_n^2 - \omega^2)^2 + (2\zeta\omega_n\omega)^2}}$$

Though $F(\omega)$ varies gradually (or even if it is a constant), $X(\omega)$ will rise rapidly near $\omega=\omega_n$. This rapid variation is due to the behavior of the denominator in the previous equation, not the numerator. Thus for example, suppose f_1=75 Hz and f_2=80 Hz and the force (or pressure) is adequately represented by linear interpolation with F_1=2 and F_2=3. Suppose further that, ζ=0.01 (1% critical damping) and $f_n=\omega_n/2\pi$=77.5 Hz. Then the structural response according to the preceding equation is as shown in the following plot, RAI 11.2. Clearly, a linear interpolation of the structural response, $X(\omega)$, between 75 to 80 Hz would be a poor approximation, though adequate for the force amplitude, $F(\omega)$, i.e., the structural response requires a finer resolution in frequency than needed for the forcing amplitude.

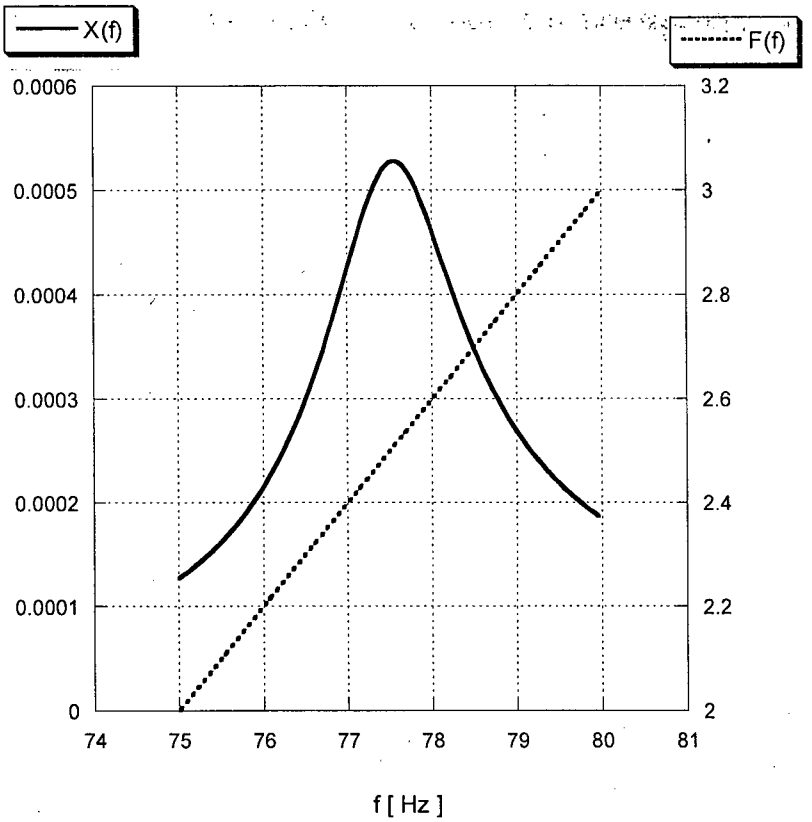

Figure RAI14.121.2. Structural response amplitude, X(f), due to linearly varying force, F(f).

(d) Section 3.3, fourth bullet: Please explain the statement, [[
]]

Response
As discussed in Section 2.3.10.p. on page 2-13 of BWRVIP-139 (BWR Vessel and Internals Project Steam Dryer Inspection and Flaw Evaluation Guidelines), during installation in the RPV, the lifting rod eyes which are threaded onto the lifting rods were adjusted for a small vertical gap with the RPV steam dryer hold down brackets and tack welded. Therefore, during normal plant operation, there is no constraint for the steam dryer from the RPV brackets.

(e) Please explain the connections of shell edges to solid faces and shell edges to solids as used in the steam dryer model and discussed in Section 3.9.

Response
Shell elements have both displacement and rotational degrees of freedom at each element node, whereas solid elements have only displacement degrees of

freedom. This raises the question of how to properly connect shell and solid elements, particularly when rotational restraints are important. For example, connecting a plate into perpendicular base modeled by solid elements would result in a simply supported plate which would be incorrect if the intended connection is a cantilever mount. To connect shells to solid elements, two procedures are used. The first pertains to cases where the shell face lies on a solid face (e.g., a flat plate lying on a solid as depicted in Fig. 6a of C.D.I. Report No. 07-17P). In this case the shell nodes are constrained to lie on the deformed solid surface, i.e., the displacement of a given shell node is given by the local solid element displacement. Shell rotations are not explicitly constrained. However, if the shell element mesh is sufficiently fine, then the constraints on displacements will automatically enforce the rotational degrees of freedom as well.

The second connection procedure is used when the shell element connects to a solid along one of the shell's edges. This connection would be used, for example, to connect the bottom edge of a vertical closure plate to the top surface of the upper support ring. In this case the shell is modified to penetrate into the solid. Specifically, the edge is extended into the solid as shown on the right with the extension modeled with additional shell elements. The penetration depth is made equal to the shell thickness, as numerical experiment has shown (DRF-PSEG-222B-F452) this value to give accurate predictions of the stresses at the junction. The displacements of the shell element nodes on the surface and the buried nodes (i.e., the shell element nodes lying inside the solid) are constrained to follow the adjacent solid element deflections. Since both the surface and buried nodes are constrained this way and these nodes are close together, rotational degrees of freedom are also effectively constrained to follow the solid deflection gradients. (See also: Cook, Robert D., "Finite element modeling for stress analysis', John Wiley&Sons, 1995. Page 118 and Fig. 5.7-2a discuss the connection of plane elements and solid elements. Page 58 and Fig. 3.9-6 discuss the connection of a beam to plane elements via extending a beam by one or two elements. In our case we extend a plate by one thickness, which is 1 or 2 plate elements inside the solid.)

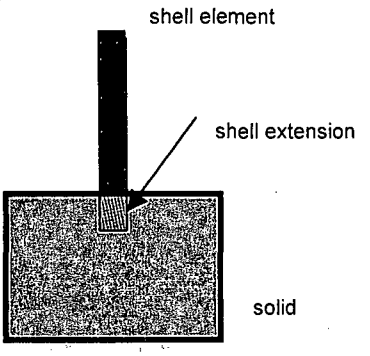

(f) In Section 4.4, the factor f_{sw} is used to reflect different weld types. Please explain the meaning of this factor and how it is used in the report.

Response

This factor is not used in the results reported in C.D.I. Report No. 07-17P (i.e., it is set to f_{sw}=1). It is provided to allow optional adjustment of the weld factor (relative to the 1.8 factor used for fillet welds) when such adjustment can be

justified. In the Hope Creek stress report, however, no such adjustment was required for any of the weld stresses and all welds used the 1.8 weld factors.

Additional RAI 14.122

According to the stress analysis using frequency based approach as documented in CDI Report 07-17P (Section 6: Conclusions), the minimum alternating stress ratio at 115 percent CLTP is 2.71 when 10 percent of the 80 Hz signal is included in the analysis. In contrast, according to the stress analysis using direct time history method as documented in CDI Report 06-27, the minimum alternating stress ratio at 115 percent CLTP is 1.33 (Table 7b). Please explain why the minimum alternating stress ratio as determined by the frequency based approach is more than twice the corresponding ratio determined using the direct time history analysis despite the inclusion of the 10 percent of the 80 Hz signal only with the frequency based approach.

Response
The difference in stress ratios is attributable to differences in structural damping, loads, and the effect of startup transients in the two analyses. Given these differences, it is reasonable to expect differences in both the values and locations of the maximum stresses in these reports.

The contribution of each of these factors to the difference in alternating stress ratios has not been calculated. However a detailed quantitative comparison of the transient and harmonic methods is provided in the response to RAI 14.110. This comparison shows that for identical structural models (including the damping model) with sufficiently small time step and sufficiently long simulation times, the transient and harmonic analyses produce identical results. The comparison also examines the differences resulting from the use of different damping models and the presence of startup transients in the response.

The differences in the predicted stresses (and hence also the stress ratios and their locations) of CDI Report 06-27, Rev. 2 and CDI Report 07-17P can be attributed to the following:

(i) Different damping models are used. The transient calculations in CDI Report 6-27 utilized a Rayleigh damping model with pin frequencies (where 1% damping is enforced) of 10 Hz and 150 Hz. Between these two frequencies the damping is lower, reaching a minimum of 0.48% at 38.7 Hz. Since response peaks scale as $1/\zeta$ where ζ is the damping ratio, it follows that in the 10-150 Hz range where the Rayleigh damping is less than 1% the associated response peaks will generally be higher than those obtained with the harmonic analysis where 1% damping is enforced throughout the frequency range. This is confirmed in the response to RAI 14.110 where the lower damping values associated with the Rayleigh damping led to higher stresses than when using 1% damping throughout the frequency range. The use of

Rayleigh damping is over conservative because some damping values are much less than the 1% typically assumed in this type of anaylisis.

(ii) The time domain calculation admits transient overshoots that incur higher estimates of both maximum and alternating stress intensity (again the response to 14.110 provides such examples).

(iii) The loads used in the two calculations were different. The results in CDI Report 06-27, Rev. 2 corresponded to 115% CLTP 1/8-th scale model loads whereas the results in CDI Report 07-17P corresponded to CLTP plant loads. The dominant component in the scale model loads (after removal of the 80 Hz signal) is a peak at approximately 120 Hz, not present in the CLTP plant loads. As such the amplitudes and frequency contents of the two loads (and consequently also the stress response) were different resulting in different high stress magnitudes and locations.

(iv) The loads in the time domain simulation and harmonic analysis were applied over different time intervals. Specifically, to contain computational costs in the time domain calculation the loads were applied to the dryer for a duration of 2 seconds. This 2 second window was taken from a longer 105 second sample by identifying when the acoustic pressure signal was a maximum and then centering the window about this maximum. For the harmonic calculation it is possible to retain the complete 105 second range.

Additional RAI 14.123

The weld locations having the lowest alternating stress ratios as reported in Tables 7b and 8b in CDI Report 07-17P (frequency based approach) appear to be different than those reported in Table 7b in CDI Report 06-27 (direct time history analysis). Please provide justification for these differences.

Response

The differences in the high stress locations are explained in the response to RAI 14.122.

References

1) Letter from George P. Barnes (PSEG Nuclear LLC) to USNRC, September 18, 2006

2) Letter from USNRC to William Levis (PSEG Nuclear LLC), November 13, 2007

ATTACHMENT 4

Hope Creek Generating Station

Facility Operating License NPF-57
Docket No. 50-354

Extended Power Uprate

Methodology to Determine Unsteady Pressure Loading on Components in Reactor Steam Domes
C.D.I. Report No. 04-09NP, Revision 6